MULTIDITHER ADAPTIVE ALGORITHMS

J.E. Pearson, S. Hansen, M.L. Minden, and C. Yeh

Hughes Research Laboratories

3011 Malibu Canyon Road

Malibu, CA 90265

September 1976

Contract F30602–76–C–0022

Interim Technical Report No. 2

For Period 1 November 1975 Through 30 June 1976

Approved for public release; distribution unlimited

Prepared For

DEFENSE ADVANCED RESEARCH PROJECTS AGENCY

1400 Wilson Boulevard

Arlington, VA 22209

Monitored By

AIR FORCE SYSTEMS COMMAND

Rome Air Development Center

Griffiss Air Force Base, NY 13441

Effective Date of Contract	1 August 1975
Contract Expiration Date	31 July 1976
Amount of Contract	$190,745,00
Contract Number	F30602-76-C-0022
Principal Investigator	J. E. Pearson (213) 456-6411, ext. 283
RADC Project Engineer	Robert F. Ogrodnik (315) 330-4306
ARPA Order No.	1279, Amendment No. 29

UNCLASSIFIED

SECURITY CLASSIFICATION OF THIS PAGE (When Data Entered)

REPORT DOCUMENTATION PAGE		READ INSTRUCTIONS BEFORE COMPLETING FORM
1. REPORT NUMBER	2. GOVT ACCESSION NO.	3. RECIPIENT'S CATALOG NUMBER
4. TITLE (and Subtitle) MULTIDITHER ADAPTIVE ALGORITHMS		5. TYPE OF REPORT & PERIOD COVERED Interim Tech. Report 2 1 Nov. 1975 - 30 June 1976 6. PERFORMING ORG. REPORT NUMBER
7. AUTHOR(s) J. E. Pearson, K. M. Brown, M. L. Minden, K. D. Price, and C. Yeh		8. CONTRACT OR GRANT NUMBER(s) F30602-76-C-0022
9. PERFORMING ORGANIZATION NAME AND ADDRESS Hughes Research Laboratories 3011 Malibu Canyon Road Malibu, CA 90265		10. PROGRAM ELEMENT, PROJECT, TASK AREA & WORK UNIT NUMBERS 6E20; 1279, Amendment 29
11. CONTROLLING OFFICE NAME AND ADDRESS Defense Advanced Research Projects Agency 1400 Wilson Boulevard Arlington, VA 22209		12. REPORT DATE Sept. 1976 13. NUMBER OF PAGES 64
14. MONITORING AGENCY NAME & ADDRESS(if different from Controlling Office) Air Force Systems Command Rome Air Development Center Griffiss Air Force Base, NY 13441		15. SECURITY CLASS. (of this report) UNCLASSIFIED 15a. DECLASSIFICATION DOWNGRADING SCHEDULE

16. DISTRIBUTION STATEMENT (of this Report)

Approved for public release; distribution unlimited

17. DISTRIBUTION STATEMENT (of the abstract entered in Block 20, if different from Report)

18. SUPPLEMENTARY NOTES

19. KEY WORDS (Continue on reverse side if necessary and identify by block number)

COAT, Adaptive Optics, Thermal Blooming Compensation, Irradiance Tailoring, Computer Simulation, Deformable Mirrors

20. ABSTRACT (Continue on reverse side if necessary and identify by block number)

The use of Zernike-polynomial modal-control coherent optical adaptive techniques (COAT) in a multidither adaptive optical system has been studied analytically. The studies have defined those modes which will be implemented into an experimental COAT system for studying thermal blooming compensation. No apparent advantage in degree of phase correction has been established for modal versus zonal multidither control.

DD FORM 1 JAN 73 1473 EDITION OF 1 NOV 65 IS OBSOLETE

UNCLASSIFIED

SECURITY CLASSIFICATION OF THIS PAGE (When Data Entered)

A 37-element, all-beryllium, deformable mirror has been constructed. Preliminary tests show a surface deformation sensitivity of 0.28 μm/150 V and a usable frequency response to 30 kHz.

Corrected irradiance-tailoring results reaffirm an earlier conclusion that thermal blooming is best minimized by making the transmitter aperture as large as possible and the irradiance distribution as uniform as possible.

3772

SCANNING PROCESSING SHEEET

PROPERTY STAMP _____

COPYRIGHTED

YES (GREEN DOT) _____ NO ✓

DISPOSITION

	SCANNED COPY	COPY 2+
HIGH USE (RED DOT)	_____	_____
ARCHIVE (YELLOW DOT)	✓	_____
DISCARD (BLUE DOT)	_____	_____

CLASSIFICATION

U2 ✓ UL_____ CLASSIFIED_____

RESTRICTION STATEMENT

YES _____ NO ✓

SEARCH

DTIC ACCESSION NUMBER: _____
(ATTACH COPY OF STINET OR DROLS RECORD)

PUBLICATION DATE > 1/1/95

YES _____ NO _____

ELECTRONIC FULL TEXT AVAILABLE

STINET_____

DROLS _____

INTERNET _____

SCANNING

DTIC ✓ TIC _____ Internet _____

BASIS/ACCESS CORRECTIONS REQUIRED

YES _____ NO _____

NUMBER OF IMAGES TO SCAN _____

File Name:C:\Mydocuments\ScanProc.doc
Revised 1/28/98

TABLE OF CONTENTS

LIST OF ILLUSTRATIONS

SUMMARY

The objective of this program on coherent optical adaptive techniques (COAT) is to investigate algorithms and techniques that can reduce the beam distortions caused by thermal blooming. This report covers the contract period from 1 November 1975 through 31 Mary 1976. The work during this period has centered on the construction and preliminary testing of a deformable mirror and associated electronics.

The construction of a 37-element, all-beryllium deformable mirror has been completed. Final polishing of the mirror is still not complete because of the inability of a supplier to deliver the bulk of the 37 piezoelectric-stack driver elements. Only 19 of the 37 stacks have been installed at this writing. Some preliminary tests on the mirror have determined its excursion sensitivity, influence function, and frequency response. At present, the mirror delivers only 0.28 μm of surface motion for 150 V of drive, slightly less than one half the design goal. The frequency response shows some unusual resonance behavior, but is usable to at least 30 kHz. The influence function has a shape given by $IN(r) = \exp(-Br^{1.5})$ and has a value of IN = 0.23 at the center of the adjacent actuator. The faceplate will be cut thinner to reduce this value to about 0.15.

The computer simulation studies of irradiance tailoring reported in the previous report were continued to correct an error in the results presented there. The basic conclusion is unchanged, however: the best way to reduce thermal blooming is to increase the transmit aperture size and make the beam as uniform as possible.

We have completed construction of high-voltage mirror drivers and a dither injector for use with the deformable mirror. Construction has begun on a 14-function Zernike polynomial generator. Computer simulation studies have identified which Zernike polynomials make the greatest contribution to blooming compensation. A computer code has been developed that provides data on generating Zernike-polynomial mode shapes with a finite number of deformable mirror elements with minimum mean square error between the actual Zernike shape and the mirror-produced surface.

During the next period the deformable mirror construction and characterization will be completed. The Zernike-polynomial generator will be completed, and performance tests will begin with the deformable mirror in the DARPA/RADC COAT system.

Publication Review

This technical report has been reviewed and is approved.

Robert F. Ogrodnik
RADC Project Engineer

I. INTRODUCTION

A. Program Objectives

The primary objective of this program on coherent optical adaptive techniques (COAT) is to analyze and experimentally demonstrate adaptive multidither correction algorithms that can reduce beam distortions caused by thermal blooming. The use of fixed transmitter intensity profiles for reducing thermal blooming will also be investigated.

B. Research Program Plan

The research program utilizes the 21-channel DARPA/RADC experimental COAT system built and tested on contracts F30602-73-C-0248 and F30602-75-C-0001. Computer simulation codes developed on these contracts and on other programs (e.g., NSWC contract N60921-74-C-0249) have been used for the analytical portions of this contract. These codes model the operation of several types of COAT servomechanisms as well as the time-dependent propagation of optical beams in an absorbing and turbulent medium. The experimental investigations require construction of a deformable mirror for the COAT system as part of the program.

To accomplish the objectives of this contract, a 12-month research program consisting of three major tasks was developed. Task 1 is an analytical task and is largely completed. Task 2 provides for the construction of a deformable mirror and is also nearly complete. In Task 3 we will use this mirror to study thermal blooming compensation with zonal multidither control and with modal control using Zernike-polynomial modes.

Amendment No. 1 to the contract has provided funds to characterize the beryllium deformable mirror being built and to assess the applicability of this design to high-power laser COAT systems. The characterization of the mirror will occur prior to the start of Task 3.

II. TECHNICAL ACCOMPLISHMENTS

A. Zernike Polynomial COAT (ZEP-COAT)

At the beginning of this program, we had some hope that multidither control of Zernike polynomial functions (modal control) might produce a greater degree of compensation for thermal blooming than localized (zonal) control of the transmitted phasefront. As a result of our computer simulation work and experimental results at Hughes and at Lincoln Laboratory, and through a better understanding of the limitations of phase compensation of thermal blooming, we no longer believe that modal control has any inherent advantage over zonal control in the degree of compensation that it can produce. This conclusion is certainly true for turbulence compensation using Zernike polynomial modal control, as shown by the results in Figure 1. For turbulence compensation, it is the number of control channels (number of degrees of freedom) that counts, not what functions are controlled.

For thermal blooming, however, it may be possible to obtain significant blooming correction with far fewer control channels than with a zonal control system. The results of Figure 1 also indicate that significant turbulence correction is possible with a limited number of Zernike control channels. With fewer channels the complexity of the control system is reduced, and faster servo response is possible when the dither mirror response limits the servo bandwidth. This last conclusion results from the computer-determined result that the maximum servo bandwidth, $(f_s)_{max}$, for a given number of sine/cosine dither channels, N_c, is given by

$$(f_s)_{max} = \frac{f_{max}}{10 + 1.6\,(N_c - 2)} \quad , \tag{1}$$

where f_{max} is the maximum dither frequency allowed by the deformable dither mirror. Note that N_c in Eq. (1) is the number of control channels,

5225–11

CURVE	ERROR REMOVED,* ORDER n Δn	ABERRATIONS REMOVED
a		NO CORRECTION (REF. 11)
b	$\Delta 3$	TILT
c	$\Delta 4$	TILT, FOCUS
d	$\Delta 6$	TILT, FOCUS, ASTIGMATISM
e	$\Delta 8$	TILT, FOCUS, ASTIGMATISM, COMA
f	$\Delta 11$	
g	$\Delta 21$	
h		37 ELEMENT COAT
i		61 ELEMENT COAT

*SEE R. J. NOLL, J OPT SOC AM 66, 207 (1976)

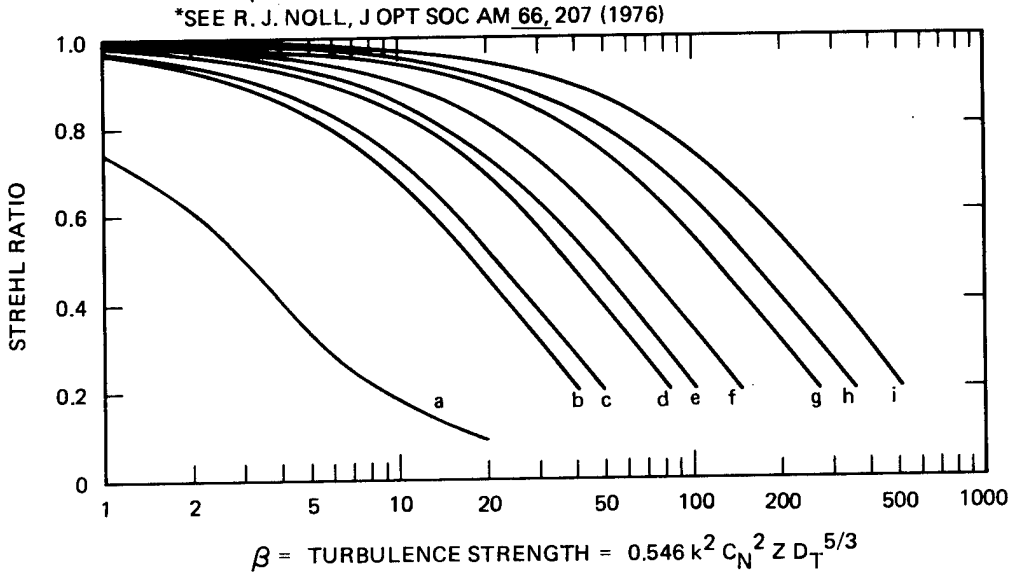

Figure 1. Analytical comparison of turbulence compensation with Zernike polynomials and zonal COAT control. The transmitter diameter is D_T.

not the number of dither frequencies (one half of N_c in a sine/cosine system), and N_c is assumed to be a multiple of 2.

In principle, a multidither COAT system can operate with any function set that is orthogonal (or nearly so) over the transmitting aperture. That is, the correction phase, ϕ_c, can be generated according to

$$\phi_c = \sum_{n=1}^{N} (a_n + \delta_n \sin \omega_n t)\, f_n(x, y) \quad , \tag{2}$$

where the two-dimensional functions f_n are orthogonal over the correction aperture, a_n are the correction amplitudes, and δ_n and ω_n are the dither amplitude and frequency for the n^{th} servo channel. For a zonal system, the functions f_n are the influence functions for the N deformable mirror actuators.

For optical systems with circular apertures, a logical choice of an alternate orthogonal correction set is the Zernike polynomials. These functions are orthogonal over a circular aperture, and the lowest-order functions are the classical aberrations of tilt, focus, coma, etc., most of which are known to have large values in phase distortions produced by turbulence and thermal blooming. We have given the name "ZEP-COAT" to a multidither modal COAT system that uses Zernike modes.

Using computer simulation codes, we have determined that only the 7 polynomials indicated with an asterisk in Table 1 are necessary for good correction in moderate thermal blooming. In determining that these 7 polynomials were the significant ones, a moderate blooming case was chosen ($P_{transmit} \approx P_{critical}$). The desired cw correction phasefront was calculated using a function-maximization routine.[a,b] This phasefront was

[a] W. P. Brown, Jr., "Computer Simulation of Adaptive Optical Systems," Final Report on Contract N60921-74-C-0249, September, 1975.

[b] J. E. Pearson, et al., "High Power, Closed Loop, Adaptive System (HICLAS) Study," Final Report on Contract N60921-76-C-0008.

Table 1. Zernike Polynomials Used in ZEP-COAT Simulation

n	Z_n	Aberration Name	β_n **
*1	X	Horizontal tilt	2
2[a]	Y	Vertical tilt	2
*3	$2R^2 - 1$	Refocus	1.5
*4	$X^2 - Y^2$	Astigmatism	3
5[a]	XY	Astigmatism	3
*6	$X(3R^2 - 2)$	Coma (Y-symmetry)	4
7[a]	$Y(3R^2 - 2)$	Coma (X-symmetry)	4
8	$X(X^2 - 3Y^2)$	120 degree (5th order, Y-symmetry)	4
9[a]	$Y(Y^2 - 3X^2)$	120 degree (5th order, X-symmetry)	4
*10	$6R^4 - 6R^2 + 1$	Spherical aberration	2.5
11	$(X^2 - Y^2)(4R^2 - 3)$	Astigmatism (5th order)	5
12	$XY(4R^2 - 3)$	Astigmatism (5th order)	5
*13	$X(10R^4 - 12R^2 + 3)$	5th order coma (Y-symmetry)	6
14[a]	$Y(10R^4 - 12R^2 + 3)$	5th order coma (X-symmetry)	6
*15	$20R^6 - 30R^4 + 12R^2 - 1$	5th-order spherical aberration	3.5

where $X = \frac{x}{\sqrt{2}} = R\cos\theta$, $Y = \frac{y}{\sqrt{2}} = R\sin\theta$, and $R = x^2 + y^2 \leq 1$

[a]These five polynomials are not used for compensating only thermal blooming because of the symmetries in the blooming distortions; the transverse wind is in the X-direction (see Ref. 11). They are used for turbulence compensation.

*Principal polynomials needed for blooming compensation.

**Relative dither amplitude for constant effective modulation index.

T1994

then fitted by means of an expansion using the first 44 Zernike polynomials. Table 2 lists the results of this calculation and Figure 2 shows the uncorrected and corrected beam profiles calculated for the conditions shown in Table 3. Although there are some contributions from higher order polynomials, their amplitudes are either less than 1/10 of the smallest amplitude among the 7 polynomials noted in Tables 1 and 2, or are of too high an order to be produced by a 37-element mirror. For the planned experiments, however, we will implement all 14 polynomials. The ZEP-COAT system can thus be used for turbulence compensation studies if so desired.

Implementing a ZEP-COAT capability into the DARPA/RADC hardware is a straightforward procedure, as indicated in Figure 3. A "polynomial generator" is merely inserted between the control channels (synchronous detectors plus low-pass filters) and the drivers for the deformable mirror. The polynomial generator is composed of several groups of weighting matrices that distribute the error signal across the mirror in the correct manner to produce the desired polynomial spatial mode. Since the dither and correction signals will be put onto a single mirror for our experiments, the low-voltage dither and correction signals will be combined, put through the polynomial box, separated and separately amplified, and then recombined onto the mirror. The process is illustrated in Figure 4.

A 14-channel polynomial generator is nearly complete; 37 mirror actuator drivers, each capable of ±150 V output, and a dither/correction combiner (dither injector) have already been completed. The interconnection of these units for either a zonal or a modal control system is shown in Figure 5. Because of the excessive delays in the delivery of the piezoelectric transducer (PZT) material for the deformable mirror (Section B of this chapter), the technical portion of the contract will be extended in time, but at no increase in cost, until the middle of November 1976 in order to complete the necessary thermal blooming studies.

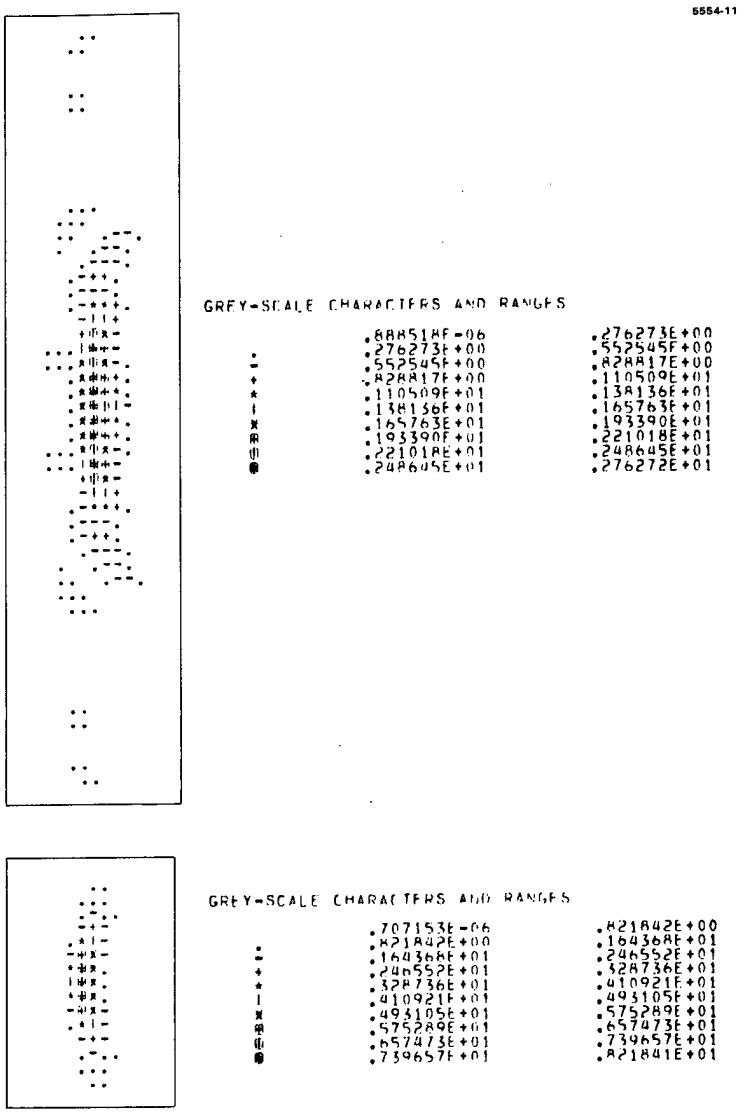

Figure 2. Thermal blooming computer simulation data for conditions listed in Table 3. (a) Uncorrected focal-plane beam profile; Strehl ratio = 0.11. (b) Corrected beam using function-maximization routine; Strehl ratio = 0.34. The phase correction used here is used to generate the Zernike polynomial amplitudes in Table 2.

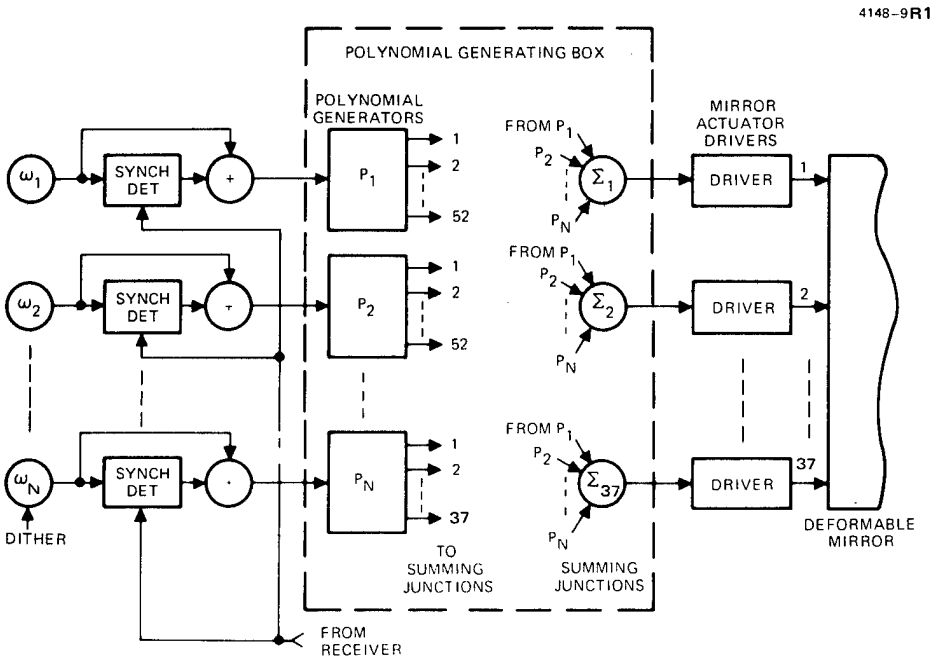

Figure 3. ZEP-COAT servo produced by adding a polynomial generating box (composed of weighting matrices P_1 --- P_N and summing junctions Σ_1 --- Σ_M) to first N-channels of a zonal multidither system.

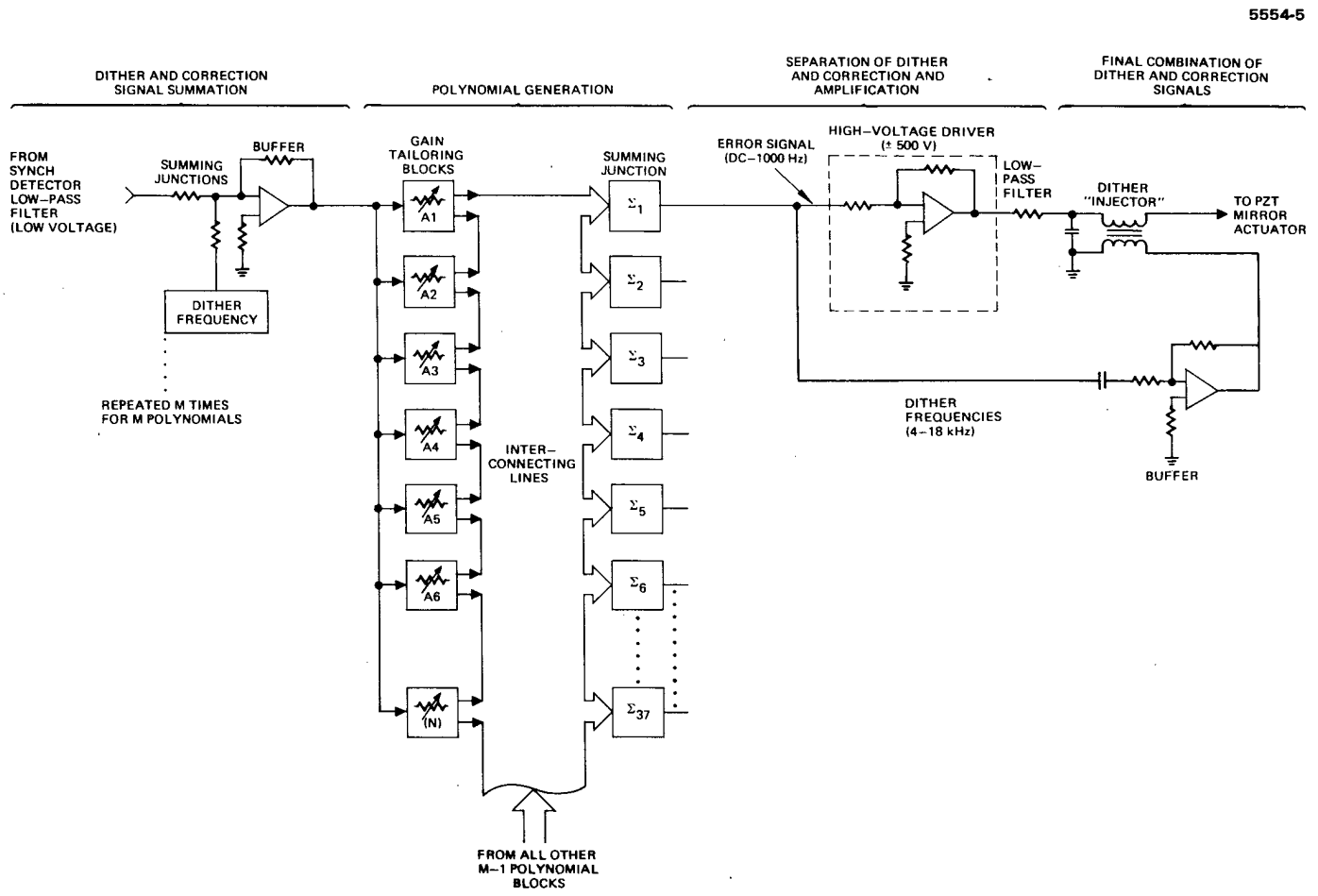

Figure 4. Zernike polynomial generator schematic for the DARPA/RADC COAT system. The dither and correction signals are combined, put through the polynomial generator, separated, amplified, and recombined.

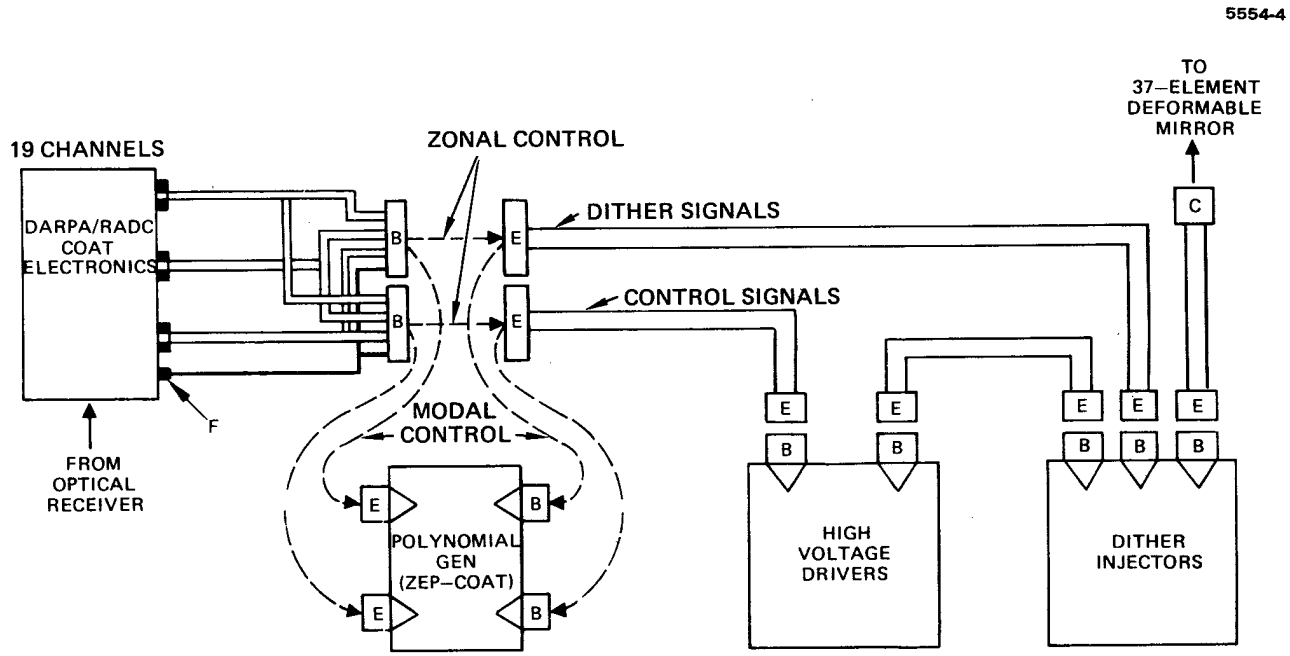

Figure 5. Wiring interconnections for DARPA/RADC COAT system using one deformable mirror for either zonal or modal control.

Table 2. Expansion of Thermal Blooming Phase Correction in Terms of Zernike Polynomials $R_n^m(\rho) \cdot \sin m\theta$ on $R_n^m(\rho) \cdot \cos m\theta$

Number	m	n	Angular Function	Radial Polynomial, R_n^m	Aberration Name	Amplitude in Blooming Correction (radians)
*1	0	2	1	$2\rho^2 - 1$	Refocus	-1.52
*2	0	4	1	$6\rho^4 - 6\rho^2 + 1$	Spherical aberration	-0.43
*3	0	6	1	$20\rho^6 - 30\rho^4 + 12\rho^2 - 1$	Spherical aberration (5th order)	-0.47
4	0	8	1	$70\rho^8 - 140\rho^6 + 90\rho^4 - 20\rho^2 + 1$		-0.59
*5	1	1	sin	ρ	y-tilt	0
*6	1	1	cos	ρ	x-tilt	-10.92
*7	1	3	sin	$3\rho^3 - 2\rho$	coma	0
*8	1	3	cos	$3\rho^3 - 2\rho$	coma	0.19
*9	1	5	sin	$10\rho^5 - 12\rho^3 + 3\rho$	coma (5th order)	0
*10	1	5	cos	$10\rho^5 - 12\rho^3 + 3\rho$	coma (5th order)	0.36
11	1	7	sin	$35\rho^7 - 60\rho^5 + 30\rho^3 - 4\rho$		0
12	1	7	cos	$35\rho^7 - 60\rho^5 + 30\rho^3 - 4\rho$		0.64
*13	2	2	sin	ρ^2	Astigmatism	0
*14	2	2	cos	ρ^2	Astigmatism	3.95
15	2	4	sin	$4\rho^4 - 3\rho^2$	Astigmatism (5th order)	0
*16	2	4	cos	$4\rho^4 - 3\rho^2$	Astigmatism (5th order)	0.53
17	2	6	sin	$15\rho^6 - 20\rho^4 + 6\rho^2$		0
18	2	6	cos	$15\rho^6 - 20\rho^4 + 6\rho^2$		0.26
19	2	8	sin	$56\rho^8 - 105\rho^6 + 60\rho^4 - 10\rho^2$		0
20	2	8	cos	$56\rho^8 - 105\rho^6 + 60\rho^4 - 10\rho^2$		-0.12
*21	3	3	sin	ρ^3	120°	0
*22	3	3	cos	ρ^3	120°	-0.38
23	3	5	sin	$5\rho^5 - 4\rho^3$		0
24	3	5	cos	$5\rho^5 - 4\rho^3$		-0.53
25	3	7	sin	$21\rho^7 - 30\rho^5 + 10\rho^3$		0
26	3	7	cos	$21\rho^7 - 30\rho^5 + 10\rho^3$		-0.62
27	4	4	sin	ρ^4		0
28	4	4	cos	ρ^4		0.27
29	4	6	sin	$6\rho^6 - 5\rho^4$		0
30	4	6	cos	$6\rho^6 - 5\rho^4$		0.71
31	4	8	sin	$28\rho^8 - 42\rho^6 + 15\rho^4$		0
32	4	8	cos	$28\rho^8 - 42\rho^6 + 15\rho^4$		1.09
33	5	5	sin	ρ^5		0
34	5	5	cos	ρ^5		-0.56
35	5	7	sin	$7\rho^7 - 6\rho^5$		0
36	5	7	cos	$7\rho^7 - 6\rho^5$		-0.67
37	6	6	sin	ρ^6		0
38	6	6	cos	ρ^6		0.58
39	6	8	sin	$8\rho^8 - 7\rho^6$		0
40	6	8	cos	$8\rho^8 - 7\rho^6$		0.30
41	7	7	sin	ρ^7		0
42	7	7	cos	ρ^7		-0.41
43	8	8	sin	ρ^8		0
44	8	8	cos	ρ^8		0.72

*To be implemented in experimental hardware.

Table 3. Assumed Conditions for Thermal Blooming Calculations

Range: 2 km	Absorption coefficient: 4×10^{-4} m^{-1}
Wavelength: 10.6 μm	Slew rate: 10 mrad/sec
Transmitter diameter: 1 m, uniform beam	Transverse wind velocity: 2 m/sec in +X direction
Resultant uncorrected Strehl ratio: 0.39	

T1996

The computer simulations being used to analyze ZEP-COAT performance were discussed in the previous contract report.[1] We also reported that we were observing an instability in the control system. We have determined that the instability was caused by an improper setting of the gain and modulation index for the channels. We have now optimized both these quantities and the ZEP-COAT servo system exhibits stable behavior under all conditions. If the dither signals applied to the mirror are represented by

$$V_d = \sum_n (\beta_n \sin \omega_n t)\, Z_n(r, \theta) \quad , \tag{3}$$

where $Z_n(r, \theta)$ are the Zernike polynomials, the the relative values of β_n for a 5% effective modulation index are given in the last column of Table 1. The values of β_n depend on the order of the polynomial according to

$$\beta_n \propto \begin{cases} \dfrac{n+1}{2} & , \quad m = 0 \\ n+1 & , \quad m \neq 0 \end{cases} \quad , \tag{4}$$

where m and n are given in Table 2.

The computer simulations have also been used to investigate multiple convergence states for ZEP-COAT systems, that is, the modal equivalents of $2N\pi$ ambiguities in zonal systems.

The $2N\pi$ ambiguity problem is normally associated only with zonal multidither systems. An analogous problem can occur with a modal ZEP-COAT system, however. That is, there exist local maxima states where the dither control system can stop (obtain a zero error signal), but which are nonoptimum for maximum focal-plane irradiance. Taken individually, the two most obvious cases are tilt (the servo can place a sidelobe of the Airy pattern on a glint) and focus.

The behavior of the focus control can be understood by referring to Figure 6. Figure 6 illustrates the well-known behavior of the on-axis intensity of a focused beam: as the focal point is approached from either direction, the on-axis intensity goes through several maxima and minima. Each maxima away from the focal plane corresponds to a different Fresnel zone, or a $2N\pi$ phase difference between rays originating from the center of the focusing lens and the outer edge. If the initial defocus is at a point such as A in Figure 6, the ZEP-COAT focus control will drive the focus toward the maximum on-axis intensity. If the starting point is at B, however, the multidither servo moves toward the nearest maximum at C and a nonoptimum target intensity results.

The problem can also exist for other Zernike functions. Table 4 lists the first 13 polynomials along with the location of the first secondary maximum and the on-axis irradiance at that maximum. At this point, we have only pointed out the potential for a servo-ambiguity for ZEP-COAT. Whether or not such ambiguities will occur in actual systems when they attempt to correct for arbitrary or random errors is a subject for future study.

We are currently setting up a computer code which will determine the relative actuator drives necessary to produce a given Zernike polynomial with a deformable mirror. This code will be used to set the values of the various resistors in the weighting matrices of the Zernike polynomial

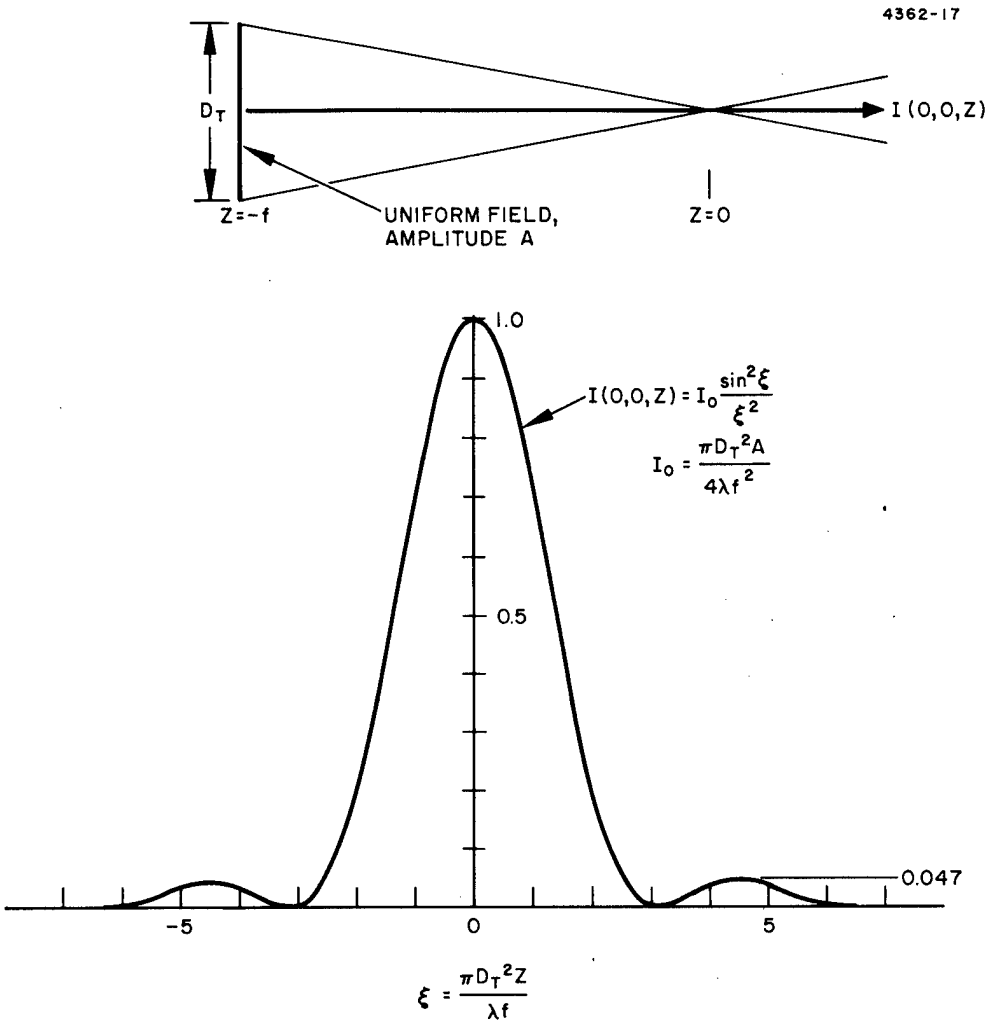

Figure 6. Behavior of on-axis intensity of a focused beam showing secondary maxima.

Table 4. $2N\pi$ Problem with Zernike Polynomials

Zernike Polynomial (Aberration)	Approximate Location of Secondary Maximum, β_i (radians)	On-Axis Intensity at Secondary Maximum Relative to that of Unaberrated Focus, I_o
1. $\psi = \beta_1(2\rho^2 - 1)$ [defocus]	4.5	$0.05\ I_o$
2. $\phi = \beta_2(6\rho^4 - 6\rho^2 + 1)$ [spherical aberration]	5.75	$0.12\ I_o$
3. $\phi = \beta_3(20\rho^3 - 3\rho^4 + 12\rho^2 - 1)$	8.7	$0.11\ I_o$
4. $\phi = \beta_4 X$ 5. $\phi = \beta_s Y$ [tilt]	5.25	$0.017\ I_o$
6. $\phi = \beta_6 X(3\rho^2 - 2)$ [coma]	Tiny one at 7.5	$0.00012\ I_o$
7. $\phi = \beta_6 Y(3\rho^2 - 2)$	Next at 12	$0.022\ I_o$
8. $\phi = \beta_8 X(10\rho^4 - 12\rho^2 + 3)$ 9. $\phi = \beta_9 Y(10\rho^4 - 12\rho^2 + 3)$	14	$0.012\ I_o$
10. $\phi = \beta_{10}(X^2 - Y^2)$ [astigmatism]	8.5	$0.022\ I_o$
11. $\phi = \beta_{11}(X^2 - Y^2)(4\rho^2 - 3)$	13.5	$0.03\ I_o$
12. $\phi = \beta_{12} X(X^2 - 3Y^2)$ 13. $\phi = \beta_{13} Y(Y^2 - 3X^2)$	None for $\beta_i \leq 25$ rad	—

T1997

generator. The best fit to a particular Z_n is a function of the mirror influence function, the number of actuators, and the interactuator spacing. Proper representation of a Z_n is necessary in order to maintain the orthogonality of the COAT-controlled functions. If the mirror cannot accurately produce the Zernike functions, the functions that are produced will not be orthogonal and the COAT control channels will be coupled together. The amount of the coupling will be a function of the rms difference between the mirror-produced function and the desired Z_n.

Another potential source of coupling with a modal system such as ZEP-COAT occurs through the amplitude distribution across the laser transmitting aperture. The polynomials listed in Table 1 are orthogonal over a uniform unit circle. For a nonuniform intensity distribution, they will not be orthogonal. If the intensity distribution is known, a new polynomial set, related to the Zernike set, can be found that is orthogonal. If the polynomials are not orthogonal, the result is again a coupling of the COAT servo channels.

Just how much channel-channel coupling a ZEP-COAT system can tolerate is not known. Previous studies of zonal systems[2,3] have shown that 20 to 30 percent coupling between channels can be tolerated in a sine/cosine dither system without noticeable degradation of performance. To our knowledge, this important problem of channel-channel coupling in a modal control system has not been satisfactorily investigated.

B. Deformable Mirror

For the experimental studies with ZEP-COAT, a 37-actuator deformable mirror is necessary, and one is being built to replace the beam-splitter/phase-shifter array (called the "phasor matrix") that has been successfully used up to now with the DARPA/RADC COAT system. The mirror will perform the two functions of phase dithering (tagging) and phase correction required in any type of multidither COAT system. Performance of both these functions with a single element places heavy and conflicting demands on the devices. The phase correction function requires

a large-amplitude phase excursion (about ±2 optical wavelengths) at relatively low frequencies (up to about 1 kHz). On the other hand, the dither function requires low-amplitude excursions ($\pm\lambda/10$) at much higher frequencies (10 to 30 kHz). To date, no continuous-surface, deformable mirror device has been constructed that can accomplish both of these functions simultaneously, particularly with the low drive voltages (±125 V) available from the DARPA/RADC COAT system.

The mirror being built on this program is the first of a kind, and as such will represent the state of the art for uncooled deformable mirrors of its type. Because such a mirror had not previously been built, or even designed, an extensive design effort was initiated. This design has been funded only in part by this contract, the remainder of the work being performed as part of the Hughes Aircraft IR&D program.

The design and analysis effort started with Hughes proprietary designs for multielement deformable mirrors and for external-spring, self-contained, piezoelectrically-driven actuator cells. The basic design and performance goals are discussed in an earlier report.[1]

A schematic of the mirror is shown in Figure 7. The entire mirror body is made of beryllium. The 37 actuators are placed on a circular array with a minimum actuator spacing of 0.550 in. The active mirror surface has a diameter of 3.980 in. The faceplate is initially 0.150-in.-thick beryllium optical stock, and is butt-brazed to each of the 37 actuators and to the rim of the primary backup. The faceplate will be polished and coated with a protective silver overcoat. The actuator cells are brazed to the primary backup at the same time as the faceplate braze.

Each piezoelectric (PZT) transducer stack is electrically grounded at the mirror faceplate and the driver voltage is applied through the electrode at the other end of the PZT stack. With this arrangement, the transducer stack is wired internally, thus eliminating the complication of feedback wires out from the stack. The only wire to each actuator is soldered conveniently to the electrode in a manner which directs the wire straight out of the cell, with no bends that require additional volume. This electrical

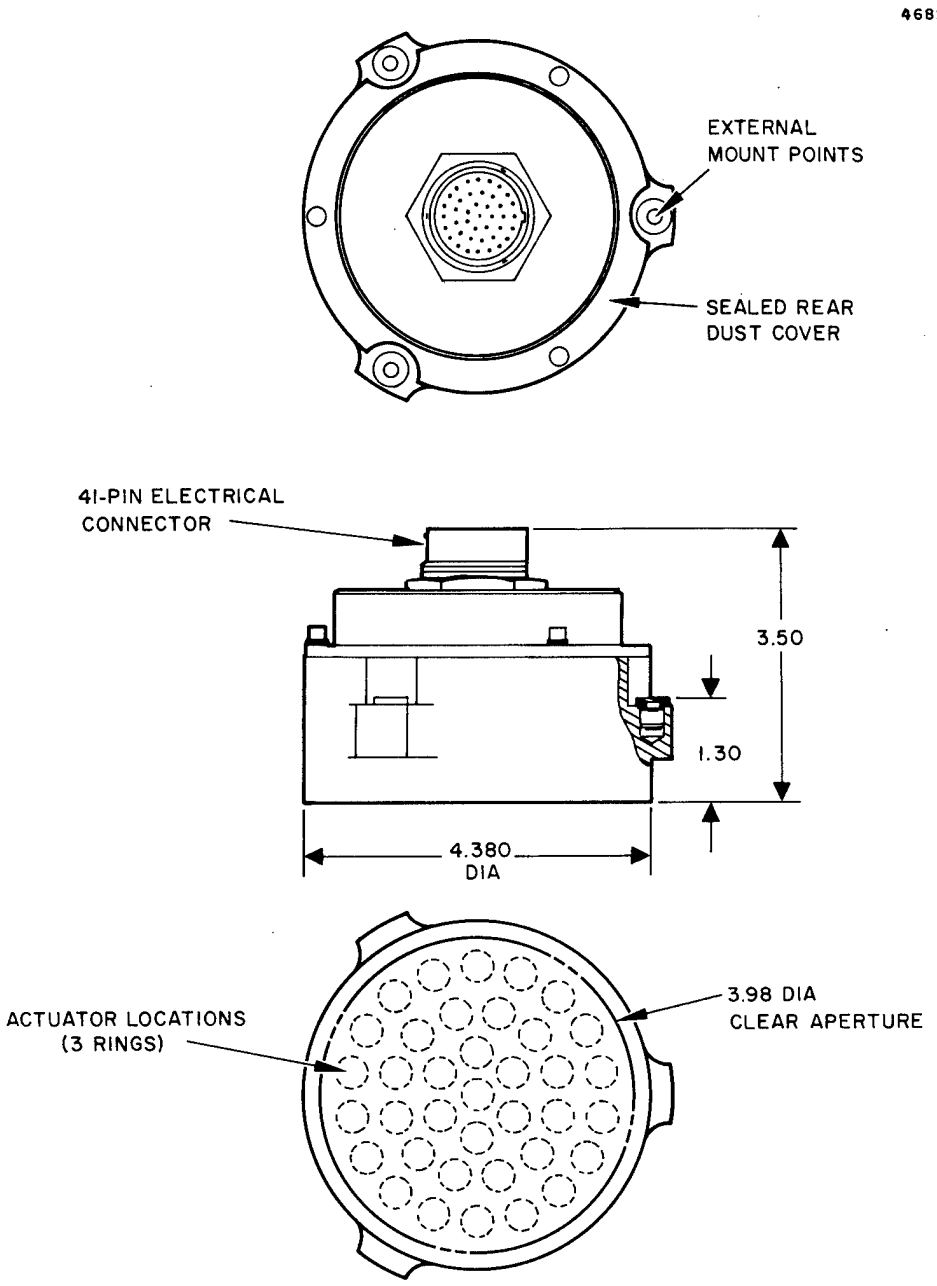

Figure 7. Schematic of 37-actuator deformable mirror designed and constructed on this contract.

arrangement is compatible with the electronics of the DARPA/RADC system, which has a common ground for all channel outputs. All of the electrical outputs are brought to a 41-pin electrical connector that is attached to the dust cover at the back of the mirror (see Figure 7).

The mirror has been fabricated and is currently being polished, although only 18 of the required 37 PZT stacks are presently available. A photograph of the unit is shown in Figure 8. An analysis performed on this mirror predicts that the lowest structural resonance will occur at 12 to 15 kHz, and appears to be a shear mode of the back-plate structure. The measured response characteristics for the central actuator (before polishing) is shown in Figure 9, with all other actuators undriven, but with preloads on them (dummy blocks were loaded into the outer ring). The response curves were obtained by placing the mirror in a Twyman-Green interferometer and looking at the surface motion of the central actuator. The response of the other actuators is similar except for some of the details of the fluctuations beyond 20 kHz. The phase of the surface response is measured relative to the sinusoidal drive voltage.

The mirror response is reasonably flat up to about 20 kHz, where a rather complicated resonance behavior beings. Using a holographic interferometer, we conclude that the fluctuations above 20 kHz are a result of excitation of complicated actuator/faceplate vibrational modes. The first two major resonances of this type were calculated to occur at 23 kHz and 40.5 kHz, in good agreement with the first two major peaks in the amplitude plot in Figure 9.

Note that the first resonance activity occurs in the neighborhood of 15 kHz, which is in good agreement with the structural analysis. The relatively small phase fluctuations indicate that the mirror is useable out to at least 30 kHz. Even a higher frequency response may be possible by filling the interior of the unit with oil, and by using lower-amplitude drive voltages at the higher frequencies (as will be done for dithers) to reduce the drive to backplate modes. At this time we do not fully understand the reasons for the enhanced amplitude response above 20 kHz.

5353-21

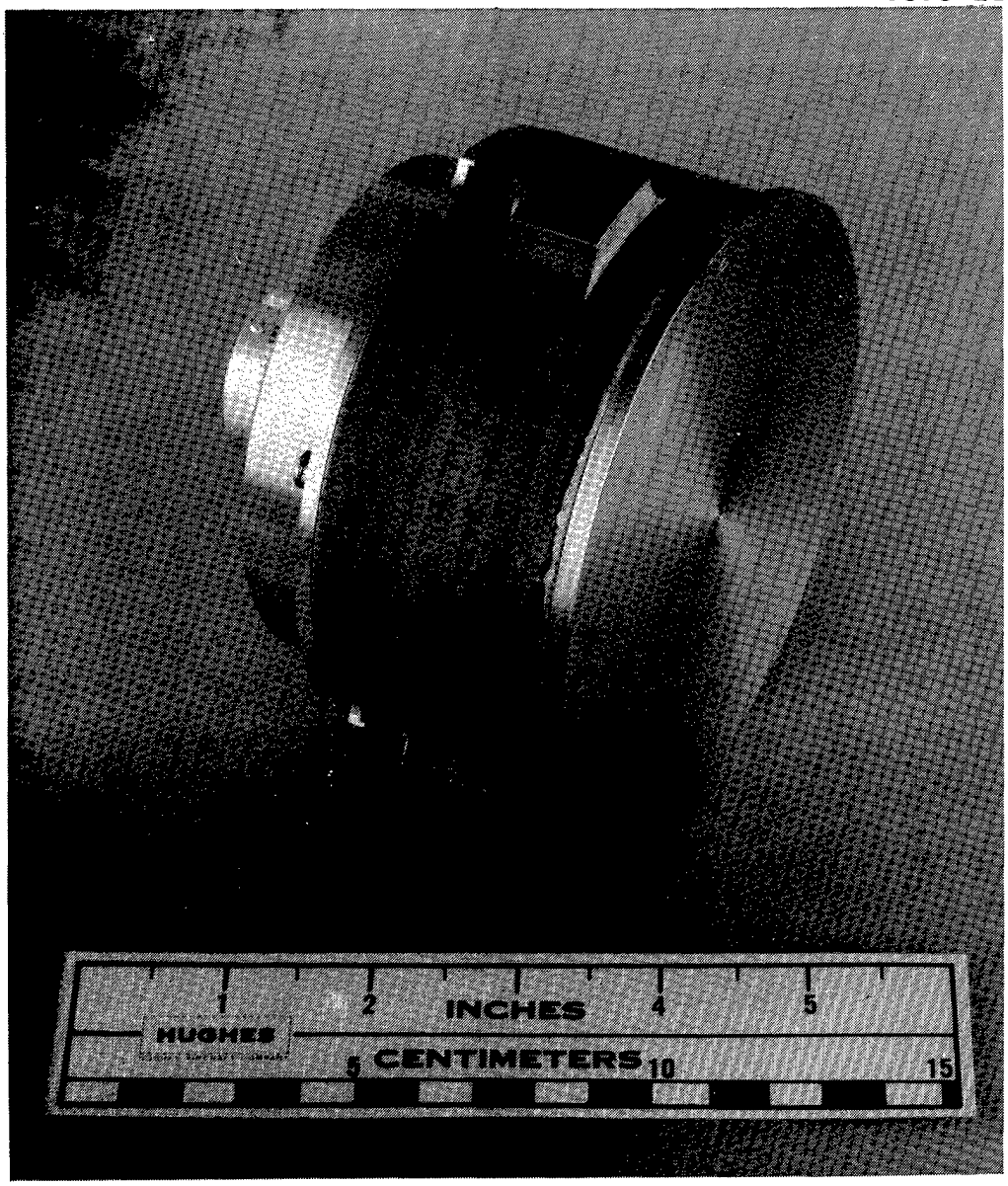

Figure 8. Photograph of 37-element DARPA/RADC deformable mirror prior to final polishing.

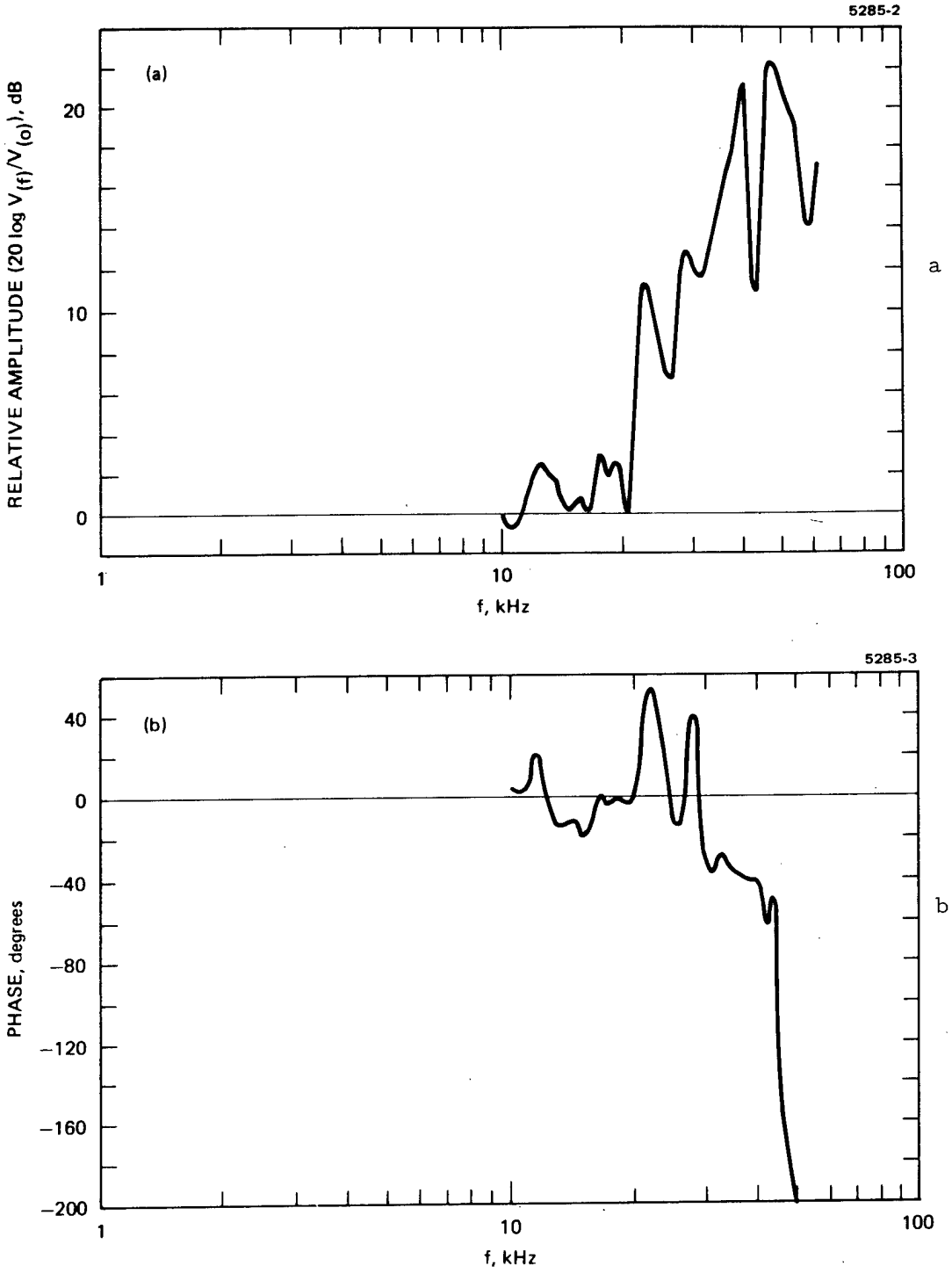

Figure 9. Measured amplitude and phase response for central actuator of DARPA/RADC beryllium deformable mirror. Drive to actuator is 42.4 V peak, producing 0.079 μm of faceplate motion.

In addition to the frequency response measurements shown in Figure 9, we have measured the influence function of an actuator in each of the 3 rings plus the central actuator. Profiles through the center of these 4 actuators are shown in Figure 10. Each actuator can produce 0.28 μm of surface motion for 150 V of drive. As can be seen, the influence function depends on the distance of the actuator from the clamped edge of the mirror; the closer to the edge, the more skewed the surface profile.

The mirror surface is measured using a simple, but highly sensitive and accurate technique. A sinusoidal drive at 500 to 1000 Hz is first applied to the appropriate actuator (or group of actuators). About 30 V rms is used, which produces a peak surface deflection of about 0.079 μm. A phonograph needle is then drawn across the surface and the resulting output is observed on an rms voltmeter as a function of the needle location. The observed profiles are repeatable to within a few percent. The technique is particularly useful because it gives the actuator influence function independent of the undriven mirror surface shape. For use on polished mirrors, the needle tip is dipped in epoxy to form a nonabrasive rounded surface. The epoxy produces very little loss in sensitivity.

As indicated in Figure 10(a), the central actuator influence function is closely approximated by the "subgaussian" function,

$$IN(r) = \exp(-3.622r^{1.5}) \quad , \tag{5}$$

where r is the radial distance in inches from the actuator center. Figure 11 shows a 3-dimensional plot of this function and Figure 12 is a contour-line plot of this profile. Notice that the profile is reasonably symmetric, but is slightly higher at the location of the actuator marked (a) than at other actuator locations.

If we define a mechanical coupling, C_m, as

$$C_m = IN(S) \quad , \tag{6}$$

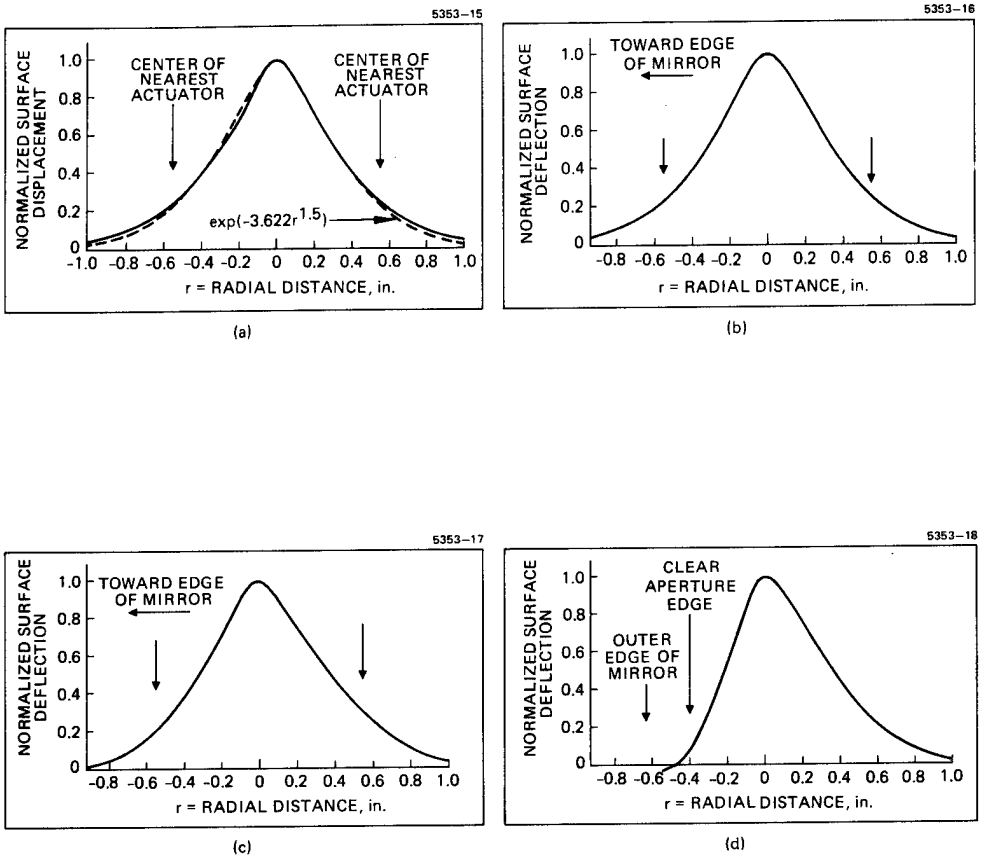

Figure 10. Influence function profiles of beryllium mirror. (a) Center actuator. (b) First ring actuator. (c) Second ring actuator. (d) Third (outermost) ring actuator. An empirical curve fit to the central actuator profile is shown as a dotted line in (a); the curve is exp $(-3.122\ r^{1.5})$, where r is the radial distance from the profile peak (actuator center) in inches. The inter-actuator center-center spacing is 0.55 in.

5353–4

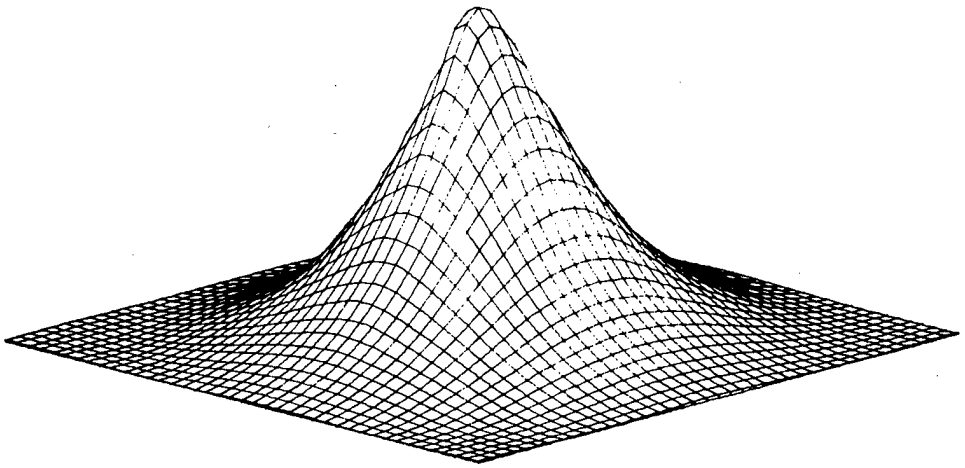

Figure 11. Three-dimensional view of centeral-actuator influence function for RADC beryllium mirror.

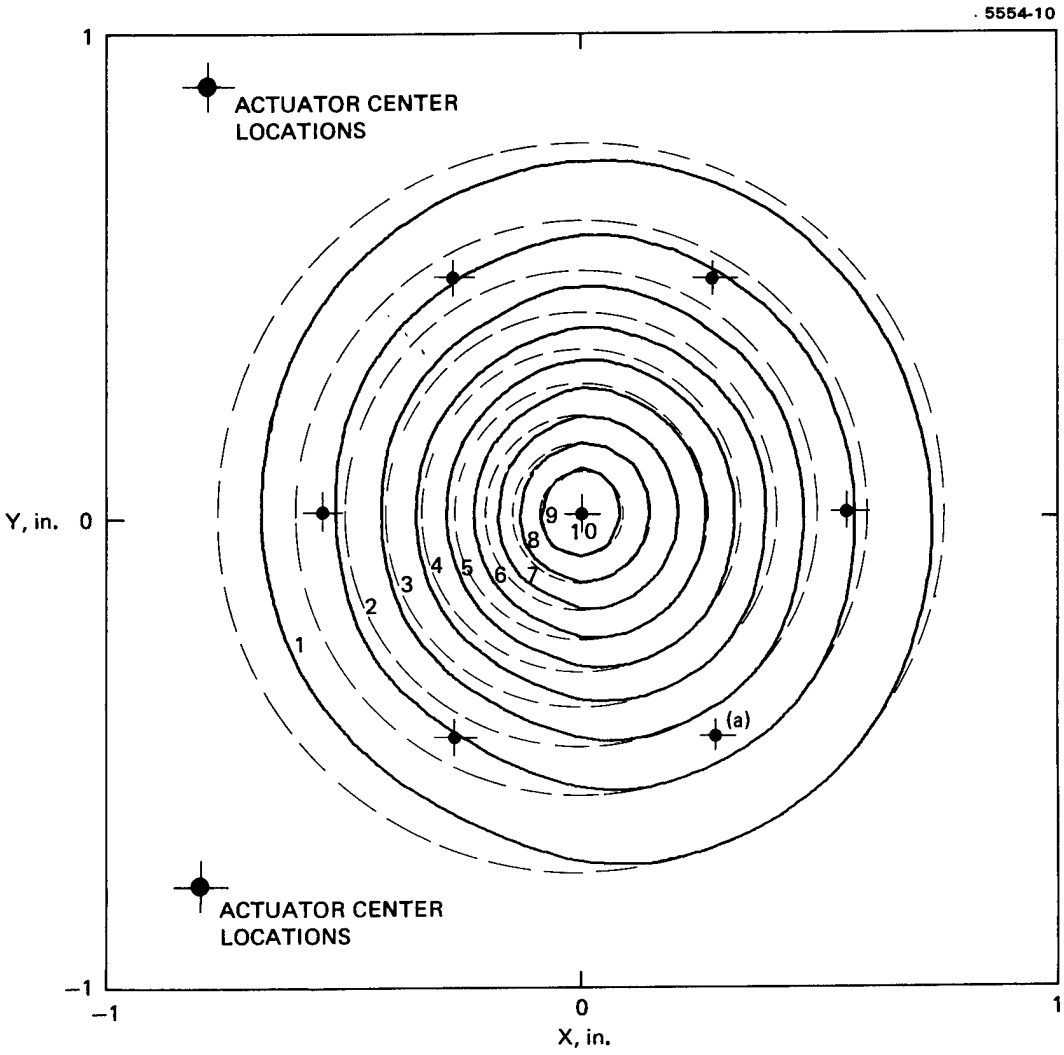

Figure 12. Contour lines of measured profile of center actuator in DARPA/RADC mirror. The locations of the actuators in the first ring are also shown. The dotted lines are circles, centered on the central actuator peak and matched to the profile contours along a line through the actuator marked (a).

where S is the interactuator center-center spacing, then $C_m = 0.23$ for this RADC beryllium mirror.

The more important quantity, however, is the servo coupling, C_{sn}. O'Meara[5] has defined this coupling as the ratio of the error signal induced in a given channel by the displacement of a single neighboring actuator to that induced by a comparable displacement of the actuator associated with the given channel. When the influence function is of the form

$$IN(r) = \exp\left[-\left(\frac{r}{r_o}\right)^n\right], \tag{7}$$

where $r^2 = x^2 + y^2$ is the squared distance from the actuator center, then the servo coupling is[4]

$$C_{sn} = \frac{n2^{2/n}}{2\pi\Gamma(2/n)} I_n, \tag{8}$$

where n is any number, $\Gamma(x)$ is the gamma function, and

$$I_n = \iint \exp\left\{-\left[x^2 + y^2\right]^{n/2} - \left[(x-\beta)^2 + y^2\right]^{n/2}\right\} dxdy. \tag{9}$$

The quantity β is given by

$$\beta = \frac{S}{r_o} = (-\ell n C_m)^{1/n}. \tag{10}$$

Reference 4 gives the values of C_{sn} for various choices of C_m and n. For the RADC mirror, $n = 1.5$ and $C_m = 0.23$, giving $C_{sn} = 0.70$. For $C_m = 0.20$, $C_{sn} = 0.67$ and if $C_m = 0.15$, $C_{sn} = 0.58$. All of these values are very substantial couplings, which may severely limit the usable COAT servo

bandwidth when this mirror is employed. This is a point which we will have to verify experimentally.

The only way to reduce the servo coupling once n is fixed, Eq. (3), is to narrow the influence function, i.e., reduce C_m. Studies conducted on the Hughes IR&D program, however, show that n = 2.0 minimizes C_{sn} for a fixed value of C_m. On the other hand, reducing C_m will increase the interactuator ripple (surface ripple when all actuators have equal excitation). The tradeoff between ripple and C_{sn} as a function of C_m is shown in Figure 13. The ripple data are obtained by calculating the surface produced by a 99-actuator, hexagonal-array mirror. Each actuator is given a unit amplitude deflection and all actuators are assumed to have the same influence function. The resulting surface is assumed to be a linear superposition of all the individual actuator influence functions. This is an approximation, but one which should be reasonably good as long as the actuator restoring springs dominate the interactuator surface "springs" caused by the faceplate stiffness (this is expected to be the case in the RADC mirror).

Note in Figure 13 that curves (b) and (c) for the ripple cross over. This implies that, for a given C_m, there is a value of n in Eq. (7) that minimizes the ripple. This optimum exponent is plotted in Figure 14 as a function of C_m. For large C_m, the value of n_{opt} approaches 2.0, a gaussian. For all cases, however, $n_{opt} > 2.0$, so the RADC mirror is expected to have a larger surface ripple when excited than a mirror with a gaussian influence function.

In fact, based on the data in Figures 13 and 14, it appears that the influence function on the RADC mirror is far from optimum. A value of n between 2 and 2.5 is desirable, with $C_m \lesssim 10\%$ so that the servo coupling will be less than 30%.

The experimentally observed surface profile when two adjacent actuators are driven with the same voltage is shown in Figure 15. For reference, the individual actuator profiles are also shown. The peak-to-peak surface ripple is 4.9% of the surface deflection at one actuator location. Figure 13 predicts 8% ripple if <u>all</u> actuators are energized. A simple superposition of 2 actuators with the same influence function,

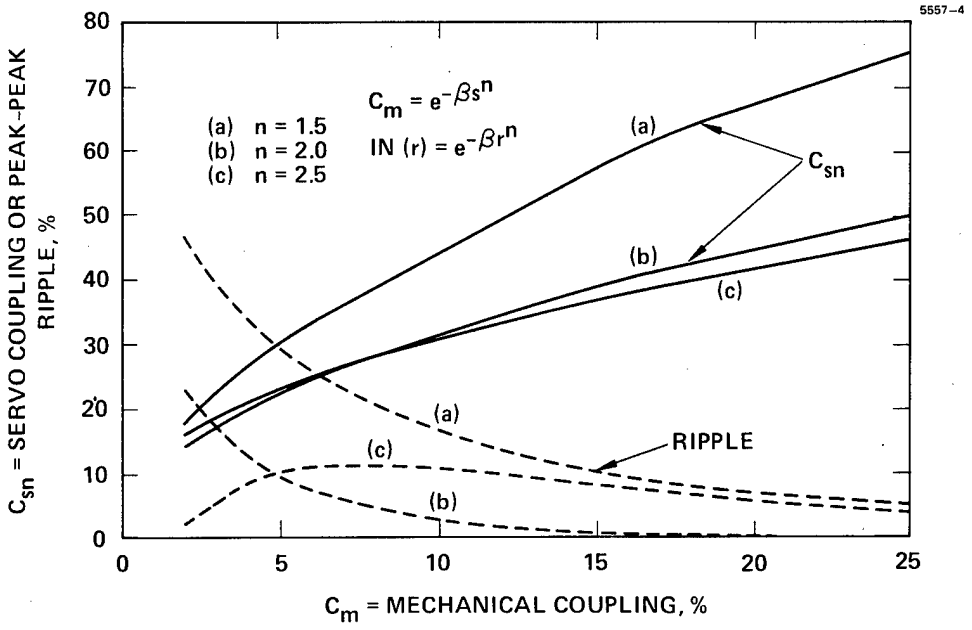

Figure 13. Servo coupling C_{sn} (eq. (8)) and peak-peak ripple as a function of deformable mirror mechanical coupling, C_m (eq. (6)). Three influence function cases are shown, a "subgaussian" (n = 1.5), a gaussion (n = 2.0), and a "supergaussion" (n = 2.5). Further data are available in Ref. 4.

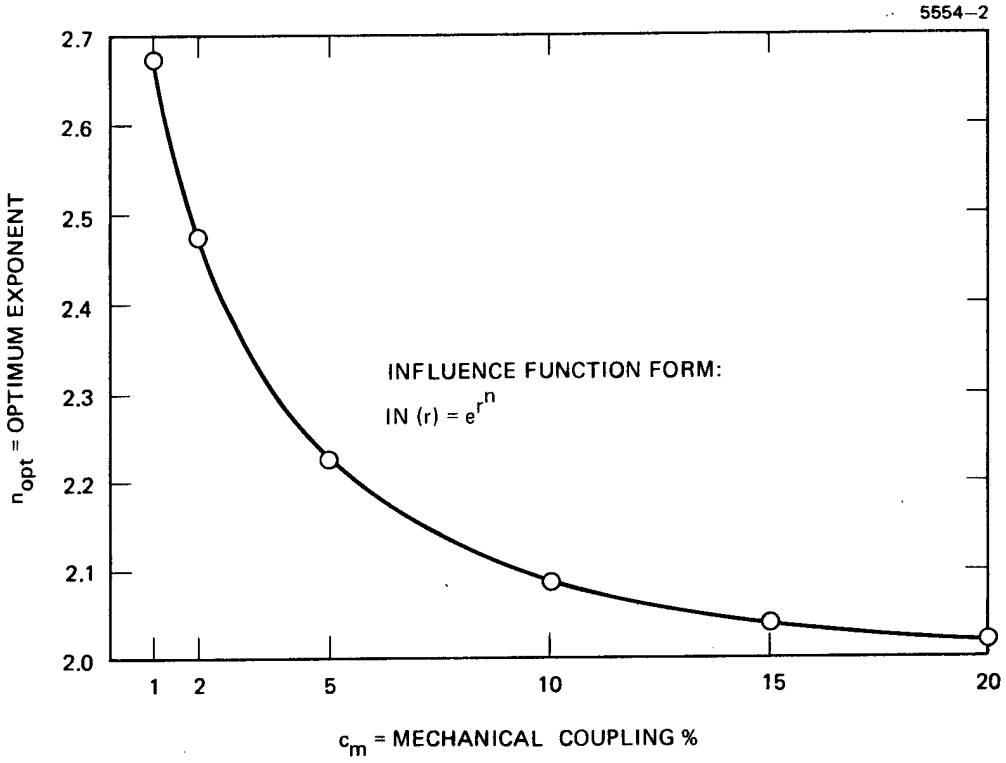

Figure 14. Optimum value of exponent, n, in eq. (3) in order to produce minimum surface ripple.

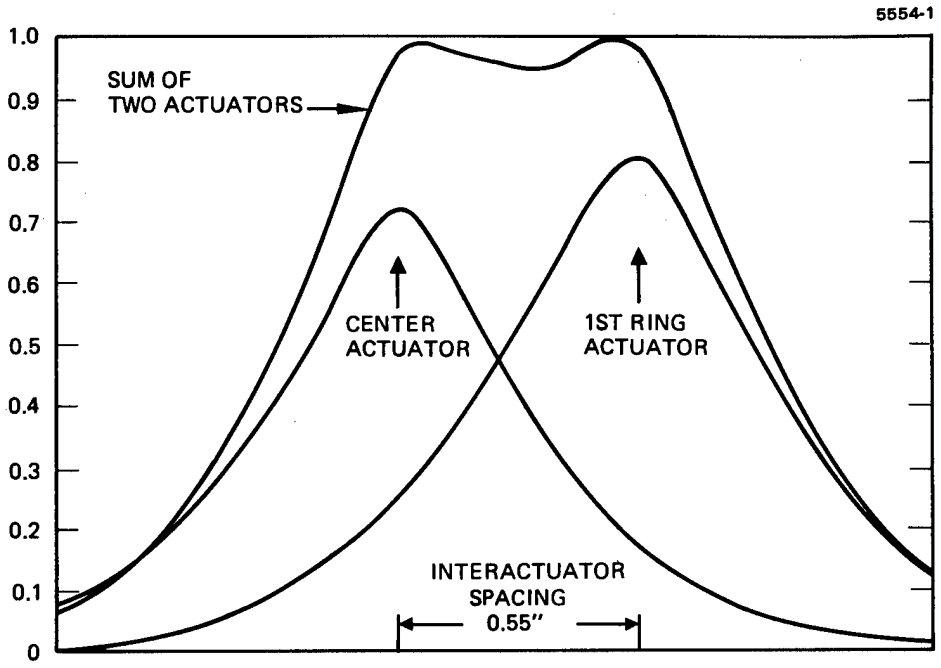

Figure 15. Experimentally observed surface profile with two adjacent actuators on DARPA/RADC mirror driven with equal voltage (≈30 V rms at 500 Hz). The individual actuator influence functions that produce the resultant surface are also shown.

$IN = \exp\left[-(r/r_o)^{1.5}\right]$, and 23% coupling, predicts a 3.3% ripple. The difference between this value and the observed 4.9% can be attributed to the differences between the two influence functions in Figure 14; they are not identical.

C. Irradiance Tailoring Studies

The previous contract report[1] presented some results on efforts to find a fixed transmitter irradiance distribution that will minimize thermal blooming effects. The basic conclusion presented there was that special laser modes and truncated distributions have little effect on the strength of blooming at a fixed transmitted power. In order to minimize blooming, the transmitter aperture should be made as large as possible and the irradiance distribution should be made as uniform as possible.

Since the time the first report was written, we have found an error in the calculations that produced Figures 7 and 10 of that report. Fortunately, the basic conclusion remains unchanged even though the quantitative output of the calculations is different. The corrected work has been accepted for publication in the Journal of the Optical Society of America, to appear in early 1977. Since the corrected results appear in that article, we present it here in its entirety as an Appendix.

III. PLANS FOR THE NEXT CONTRACT PERIOD

The next phase of the contract will be devoted almost exclusively to characterizing the RADC beryllium mirror. The faceplate will be thinned to 0.125 in. to reduce the mechanical coupling, and the unit will be polished with 19 actuators in place. All of the data required by Amendment No. 1 to the contract will be obtained. These data will form the substance of the 3rd interim report of the contract.

In addition to completing the construction and characterization of the mirror, we will also complete the Zernike polynomial generator and set up the thermal blooming optical system. Our present plans are to use a flowing-liquid blooming medium for two reasons: (1) difficulties and safety hazards with the flowing-gas cell; (2) ease of producing substantial blooming with the limited optical power available. Previous work[6-8] has indicated no signficant differences between thermal blooming produced in a gaseous or in a liquid medium.

APPENDIX

Propagation of Laser Beams Having an On-Axis Null in the Presence of Thermal Blooming

PROPAGATION OF LASER BEAMS HAVING AN ON-AXIS NULL IN THE PRESENCE OF THERMAL BLOOMING*

J. E. Pearson, C. Yeh†, and W. P. Brown, Jr.

Hughes Research Laboratories
3011 Malibu Canyon Road
Malibu, California 90265

ABSTRACT

The propagation of focused beams having an on-axis irradiance null is considered in the presence of thermal blooming. Two cases are treated: (a) beam profiles that have an irradiance zero in the beam center at the focal plane as well as the transmitter aperture; (b) beam profiles that have an on-axis irradiance null only at the transmitter. It is demonstrated that none of the beam profiles considered in case (a) has a meaningful advantage over a Gaussian beam profile. Some of the case (b) profiles do produce a larger bloomed irradiance in the focal plane, particularly when the initial intensity distribution is very uniform in its non-zero regions. Addition of a simple central obscuration to a "filled" irradiance distribution is found to have no advantage, however, for the cases considered.

---

*To be published in the Journal of the Optical Society of America. This work sponsored in part by the Air Force Systems Command's Rome Air Development Center, Griffiss AFB, NY.

† Permanent address: Electrical Engineering Department,
University of California at Los Angeles
Los Angeles, California 90024

I. INTRODUCTION

When an optical laser beam is propagated through an absorbing medium with a negative refractive index temperature coefficient ($dn/dT < 0$), the phenomenon of thermal blooming[1, 2] occurs. In the presence of thermal blooming, the propagation medium acts like a negative lens that defocuses, spreads, and distorts the optical beam. This power-dependent phenomenon can be particularly harmful when the optical system is attempting to produce maximum focal plane irradiance.

It has been suggested that the use of a transmitted beam that has an annular intensity profile may provide higher focal plane irradiance in the presence of thermal blooming[3] than that produced by a Gaussian beam. The physical reasoning behind this suggestion is straightforward. A Gaussian intensity profile produces a quadratic refractive index variation in the medium that is minimum at the beam center where most of the optical power occurs. With an annular beam that has an on-axis null, the negative lens induced in the medium has a larger refractive index on-axis than off-axis. The result is a positive lens for light that is close to the beam axis, and this lens tends to counteract some of the off-axis negative lens beam spreading as the optical beam propagates.

This article presents the results of an investigation aimed at quantifying how much thermal blooming distortions are reduced by the use of laser beam that have an on-axis intensity zero. Such beams can be produced either by apodization (truncation), or by use of laser resonators that have annular gain profiles,[4] or by many unstable resonator configurations such as those used in many high energy laser devices. The investigations were performed by computer simulation of the propagation problem. The computer code[5] solves the coupled differential equations that describe both the medium dynamics and the diffraction-propagation of a focused laser beam. Convection-dominated heat transfer produced by a transverse wind is assumed and the quantity of interest is the peak focal plane irradiance.

Two types of annular or "on-axis-null" intensity profiles are treated. Section II discusses those that have an intensity zero in the beam center,

both in the focal plane (far-field) as well as at the transmitter (near-field) and thus are free-space propagation modes. Section III discusses those profiles that have a zero in the beam center only at the initial transmitter plane. Due to diffraction, the initial on-axis null fills in as these beams propagate so that the on-axis irradiance is not zero at the focal plane. An appropriate choice of the initial profile can indeed increase the maximum focal plane irradiance. The standard of comparison in all cases is the focal plane irradiance produced by a Gaussian beam that is truncated at the 10% intensity radius.

II. "ON-AXIS-NULL" IRRADIANCE PROFILE AT THE TRANSMITTING APERTURE (NEAR-FIELD) AND AT THE FOCAL PLANE (FAR-FIELD)

In this section, we consider cases where the irradiance null in the middle of the beam is retained as the focused beam is propagated to the target. To first demonstrate that an appropriately chosen transmitter irradiance distribution can indeed be focused to produce an on-axis-null focal-plane irradiance distribution, we start with a transmitter aperture field given by[4]

$$E(r_1, \theta_1) = A_m f_m(r_1) \cos(m\theta_1), \quad (m = 0, 1, 2 \ldots .) , \tag{1}$$

where A_m is the maximum field magnitude, $f_m(r_1)$ may be a continuous or a discontinuous function of r_1, and (r_1, θ_1) are the transverse polar coordinates of the transmitting aperture. From Fresnel diffraction formulae, we obtain the field u at the focal plane:

$$u(x_o, y_o, z) = \frac{e^{jkz}}{j\lambda z} \exp\left\{ j \frac{k}{2z} \left(x_o^2 + y_o^2 \right) \right\} \cdot \iint_{-\infty}^{\infty} A(r_1, \theta_1) \exp\left\{ - j \frac{2\pi}{\lambda z} (x_o x_1 + y_o y_1) \right\} dx_1 dy_1 , \tag{2}$$

where z is the focal distance, λ the free-space wavelength, $k = 2\pi/\lambda$, (x_o, y_o) are the transverse rectangular coordinates at the focal plane, and (x_1, y_1) are the transverse rectangular coordinates at the transmitting aperture plane. Changing Eq. (2) into polar coordinates and carrying out the angular integration, we find

$$u(r_o, \theta_o, z) = \frac{e^{jkz}}{j\lambda z} \exp\left\{ j \frac{k}{2z} r_o^2 \right\} \int_0^\infty f_m(r_1) r_1 dr_1 \cdot$$

$$\cdot \int_0^{2\pi} \cos(m\theta) \exp\left\{ - j \frac{2\pi}{\lambda z} r_1 r_o \cos(\theta_1 - \theta_o) \right\} d\theta_1 \qquad (3)$$

$$= \frac{e^{jkz}}{j\, z} \exp\left\{ j \frac{k}{2z} r_o^2 \right\} 2\pi \cos(m\theta_o) e^{-j m \frac{\pi}{2}} I_m(r_o),$$

where

$$I_m(r_o) = \int_0^\infty A_m f_m(r_1) J_m\left(\frac{2\pi}{\lambda z} r_1 r_o \right) r_1 dr_1 . \qquad (4)$$

The on-axis irradiance occurs at $r_o = 0$ and is given by

$$\left| u(0, \theta_o, z) \right|^2 = \left[\frac{2\pi \cos(m\theta_o)}{\lambda z} \right]^2 I_m^2(0) . \qquad (5)$$

Since $J_m(0) = 0$ when $m \neq 0$, Eq. (4) indicates that $I_m \equiv 0$ for $m \neq 0$. An on-axis-null focal plane irradiance is thus obtained for all $m \neq 0$. When $m = 0$, however, the on-axis focal plane irradiance may take on any value, including zero, depending upon the initial radial dependence of u.

The particular transmitter irradiance profiles that we have chosen to study are given in Eqs. (6) and (7) and are illustrated in Fig. 1. The truncated Gaussian beam we are using for comparison purposes is also shown in Fig. 1 and defined in Eq. (8).

Case (II-a)

$$|u|^2 = A_1^2 \, e^{-r_1^2/\rho_o^2} \cos^2\theta_1, \quad \text{for } r_1 \le a_o \tag{6}$$

$$= 0 \qquad \text{for } r_1 > a_o$$

Case (II-b)

$$|u|^2 = A_2^2 \, e^{-\left(\frac{r_1 - r_m}{\rho_o}\right)^2 \frac{1}{\rho^2}} \cos^2\theta_1, \quad \text{for } b_o \le r_1 \le a_o \tag{7}$$

$$\text{and } b_o < r_m < a_o$$

$$= 0, \text{ otherwise}$$

Truncated Gaussian

$$|u|^2 = A_o^2 \, e^{-r_1^2/\rho_o^2}, \quad \text{for } r_1 \le a_o \tag{8}$$

$$= 0, \qquad \text{otherwise} \quad .$$

For these beams, the first two of which can be produced by coaxial-resonator, annular-gain lasers,[4] ρ_o is the e-folding intensity radius of the Gaussian beam in Eq. (8), ρ is a constant less than or equal to 1,

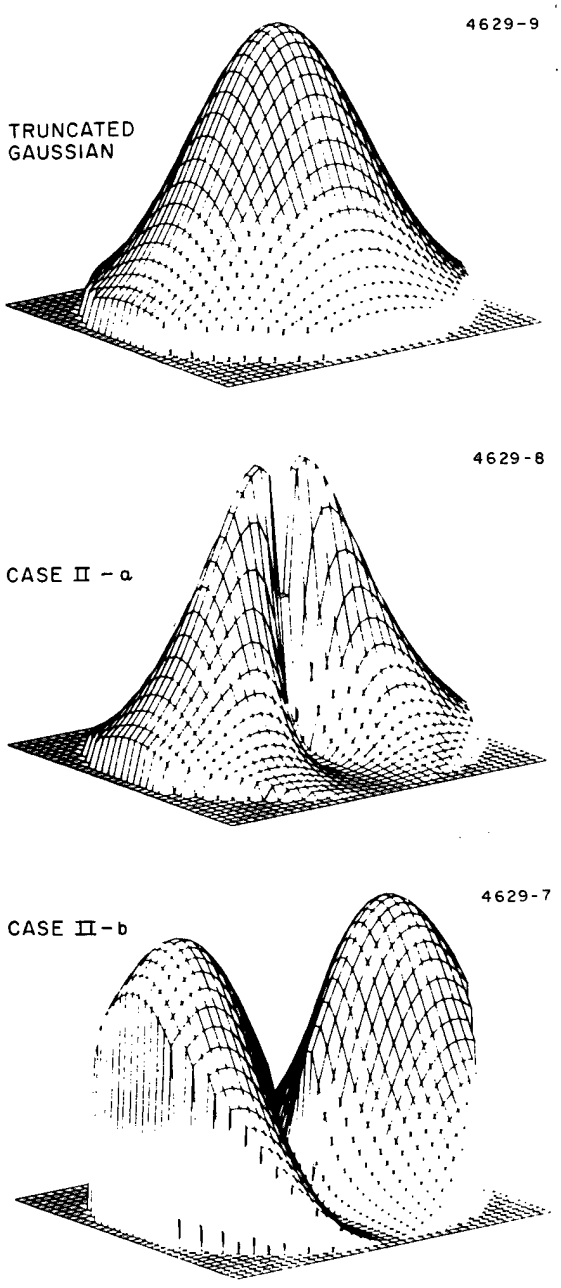

Figure 1. Three-dimensional plots of transmitter irradiance profiles that retain their shape for free-space propagation. The truncated Gaussian beam is used as a comparison reference for all other beams considered. The two "on-axis-null" profiles shown here also have an on-axis null in the focal-plane.

r_m is the adjustable maximum intensity radius, and b_o and a_o are the inner and outer radii of a coaxial laser resonator. The beams in Eqs. (6) and (7) are assumed oriented in such a way that the $\theta_1 = \pi/2$ axis is parallel to the transverse wind direction. This orientation produces minimum blooming since the heated air from one main transmitter lobe does not pass through the region heated by the other main lobe. The field amplitudes A_1, A_2, and A_3 are chosen so that the total transmitted power is constant. The expressions used to obtain these amplitudes are derived in the appendix.

Figure 2 compares the initial transmitter irradiance distributions of the three beams to the focal-plane irradiance distributions for a representative transmitter power. The parameters necessary to specify the blooming strength are given in the appendix. For all the computational results presented here, we have chosen values for the various constants to correspond to the obscuration ratio in some laser pointer/tracker systems now in use, and to give the most uniform initial intensity distribution; we have found that thermal blooming is minimized for uniform initial intensity distribution; we have found that thermal blooming is minimized for uniform initial intensity profiles. The values used in our calculations are $a_o/\rho_o = 1.52$, $a_o/b_o = 7$, $r_m/a_o = 2/3$, and $\rho = 1$. Note that in the absence of blooming effects, the focal plane distributions would look like the transmitter distributions for each case.

The peak focal-plane irradiance as a function of total transmitted laser power for these three beam cases is given in Fig. 3. Both the irradiance and the transmitter power are plotted in normalized units as discussed in the appendix. The maximum focal-plane irradiance for Case (II-b) is a factor of 1.2 larger than that obtained with the truncated Gaussian beam. The higher irradiance is obtained by increasing the total laser power at the aperture plane by a factor of 2.75. Case (II-a) yields lower peak focal-plane irradiance even with higher total laser power. Hence, no significant improvement is obtained with transmitting intensity profiles tailored according to cases (II-a) or (II-b).

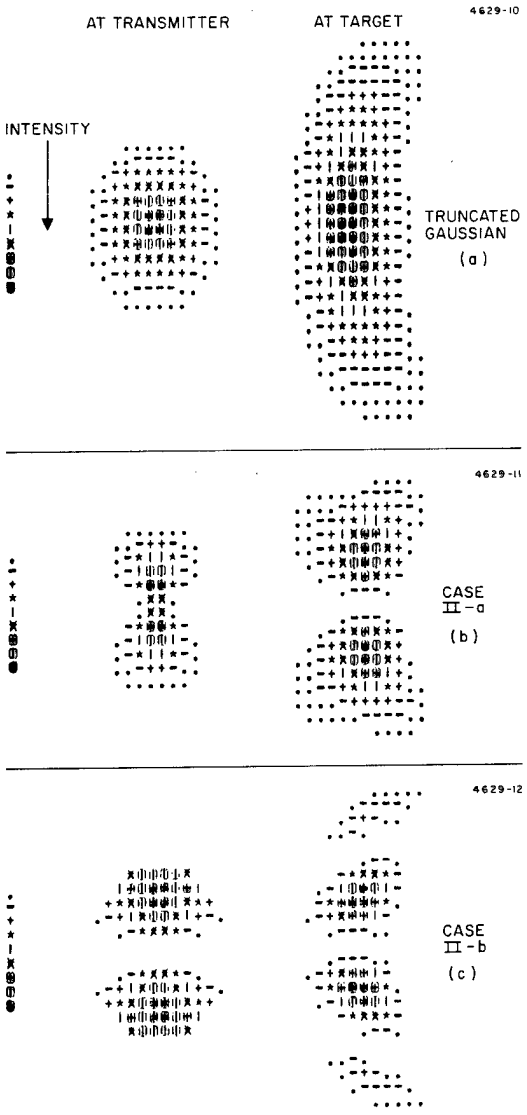

Figure 2. Pseudo-gray scale plots of transmitter and focal-plane irradiance distributions for the three beams in Fig. 1. A moderate amount of thermal blooming is present in the propagation path.

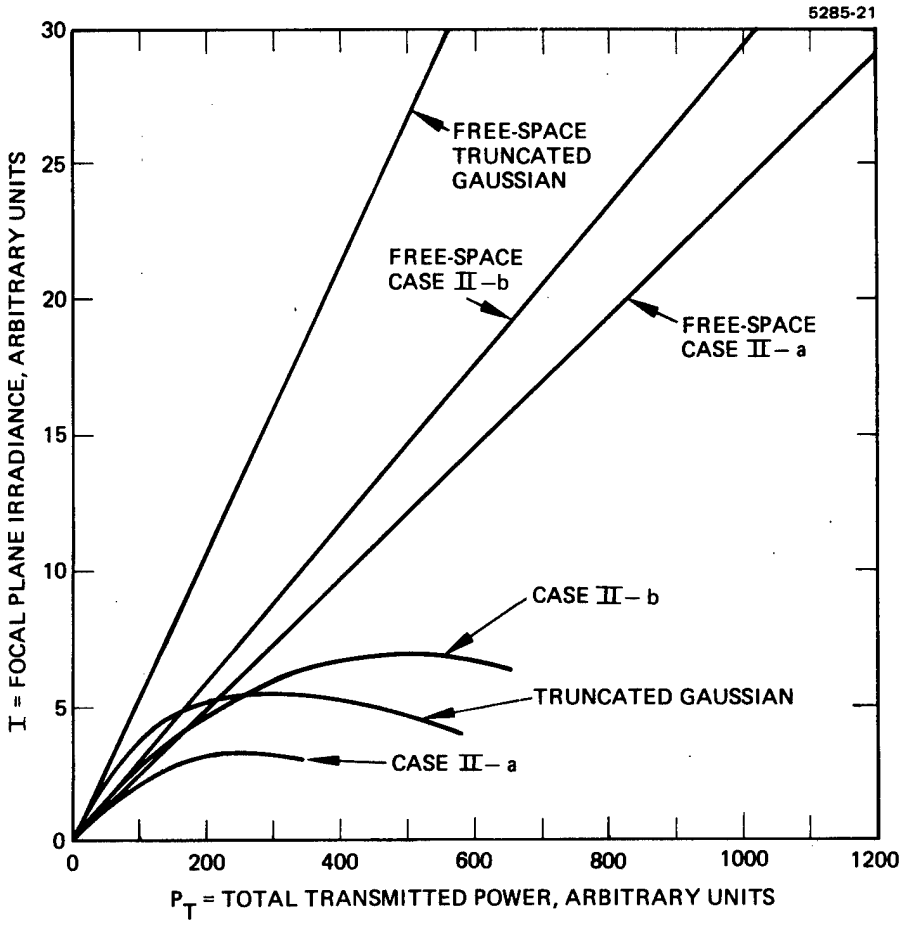

Figure 3. Peak focal-plane irradiance versus total transmitter power for the same three cases as in Figs. 1 and 2. The axis units are normalized values as discussed in the Appendix.

III. "ON-AXIS-NULL" INTENSITY PROFILE ONLY AT THE TRANSMITTING APERTURE (NEAR-FIELD)

We now treat cases for which the on-axis intensity null occurs only at the transmitting aperture. In other words, under thermal blooming conditions, the cooler region in the middle of the beam does not exist throughout the focused propagation path to the focal plane. Four specific aperture intensity profiles are considered and compared to the truncated Gaussian in Eq. (8):

$$\text{Case (III-a)} \quad |u|^2 = A_3^2 \left(\frac{r_1}{\rho_o}\right)^4 e^{-(r_1^2/\rho_o^2)} \quad , \text{ for } r_1 < a_o$$
$$= 0 \quad \text{for } r_1 > a_o \tag{9}$$

$$\text{Case (III-b)} \quad |u|^2 = A_4^2 \, e^{-(r_1 - r_m/\rho_o)^2} \frac{1}{\rho^2} \text{, for } b_o < r_1 < a_o$$
$$= 0 \quad \text{, otherwise} \tag{10}$$

$$\text{Case (III-c)} \quad |u|^2 = A_5^2 \quad \text{, for } b_o < r_1 < a_o$$
$$= 0 \quad \text{, otherwise} \tag{11}$$

$$\text{Case (III-d)} \quad |u|^2 = A_6^2 \, e^{-r_1^2/\rho_o^2} \quad \text{, for } b_o < r_1 < a_o;$$
$$= 0 \quad \text{otherwise .}$$

The beam amplitudes A_3, A_4, A_5, A_6 are chosen to keep the total transmitter power constant. The calculations for these amplitudes are given in the appendix. Computer-generated plots of the initial beam pforiles are illustrated in Fig. 4.

The transmitter aperture intensity profiles as well as the corresponding focal plane intensity profiles for these cases are displayed in Fig. 5 for a representative laser power level. Figure 6 compares the normalized peak focal plane irradiance as a function of normalized total input transmitting power for these four cases to that for the truncated Gaussian case. Unlike the cases treated in Section II, significantly larger peak focal plane irradiance is achieved for two of the four cases considered as compared with that for the truncated solid Gaussian. Case (III-d) yields a peak focal plane irradiance which is the same as that for the truncated Gaussian beam.

The intensity profile for Case (III-a) is obtained by combining the TEM_{00} and TEM^{*}_{10} modes of a cylindrical cavity oscillating in phase opposition (Laguerre-Gaussian modes[7]). The peak focal plane irradiance achieved with this profile is almost twice that of the truncated solid Gaussian beam with a total laser power roughly 2.5 times that for the truncated solid Gaussian beam. Other ways to increase focal plane irradiance by this amount such as coherent optical adaptive techniques (COAT)[8] may be more practical and efficient if this type of mode is difficult to produce in practice in high power lasers.

In cases (III-b) and (III-c), the peak focal plane irradiance is also about twice the value for the truncated solid Gaussian beam, but as shown in Fig. 6, this increase is obtained at about 90% of the total input laser power of the truncated solid Gaussian beam. A very uniform intensity distribution is thus desirable for reducing blooming, but may be very difficult to obtain in practice.

IV. CONCLUSION

These results lead us to conclude that many special laser modes or intensity distributions that have an on-axis null or minimum do not offer

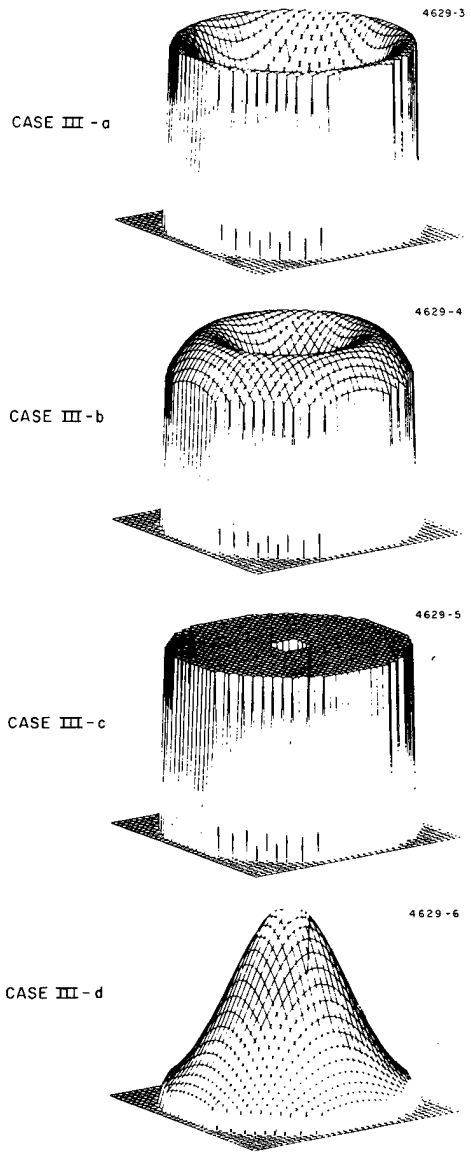

Figure 4. Three-dimensional plots of transmitter irradiance profiles that have an on-axis null initially that fills in as the beams propagate. Case III-a is a mixture of cylindrical modes TEM_{00} and TEM_{01} oscillating in phase opposition. Case III-b is similar to Case II-b, except $|u|^2$ has no θ-dependence. Case III-c is a uniform annular beam. Case III-d is an annularly-truncated Gaussian beam.

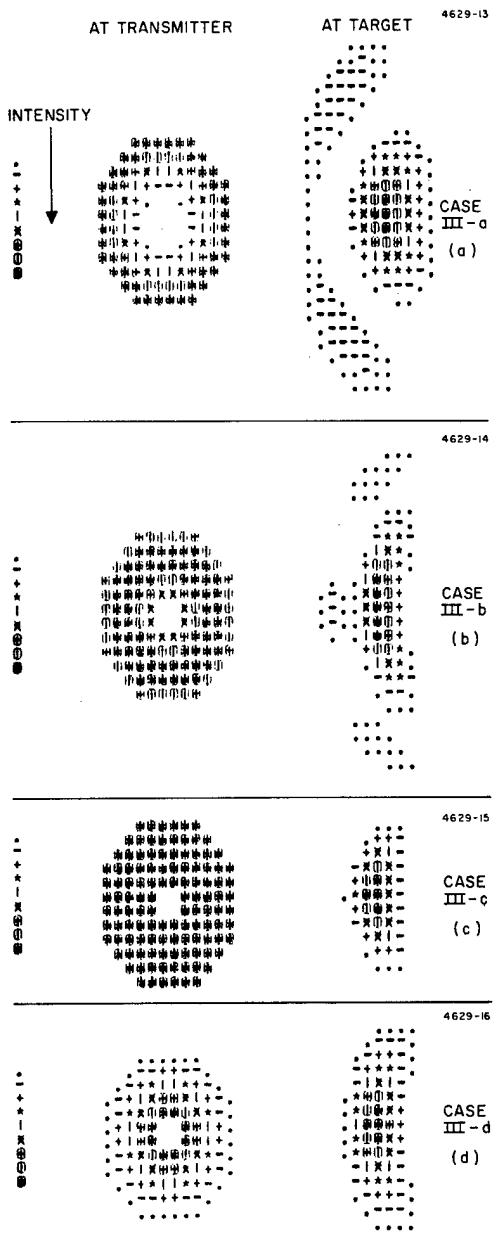

Figure 5. Pseudo-gray scale plots of transmitter and focal-plane irradiance distributions for the three beams in Fig. 4. A moderate amount of thermal blooming is present in the propagation path.

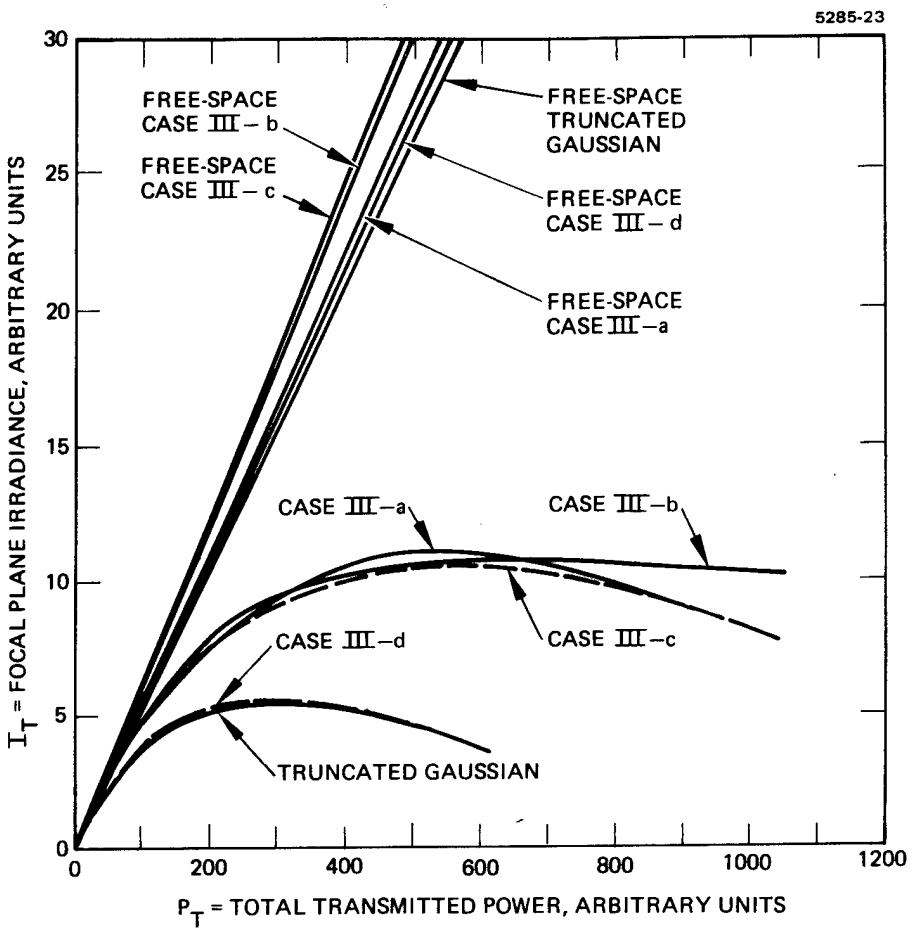

Figure 6. Peak focal-plane irradiance versus total transmitter power for the four beams in Figs. 5 and 6. The axis units are normalized as discussed in the Appendix.

any significant advantages for reducing thermal blooming when the goal is to achieve maximum focal-plane irradiance for a given transmitter power. In particular, the laser modes considered here that produce an on-axis null in both the near-field and far-field have no advantages over intensity distributions that have the null only in the near-field of the transmitter. Significantly less blooming does occur, however, for certain annular, circularly symmetric laser modes and for initial irradiance profiles that are very uniform in the non-zero regions (a uniform annulus, for example).

One question that is frequently asked is whether the "holes" introduced into beams by unstable resonators should be eliminated or whether they may provide some advantage. Although we have not considered a sufficient number of cases to make a definite conclusion, our studies to date of filled beams and of beams with a central hole or obscuration indicate that the hole makes very little difference, at least as far as thermal blooming is concerned. When the goal is to minimize thermal blooming distortions so that maximum focal-plane irradiance is achieved, then it is much more profitable to force the initial beam intensity profile to be as uniform as possible in its non-zero regions rather than attempt to produce or eliminate central holes in the beam. Increasing the initial transmitted beam diameter is also quite effective in reducing blooming distortions, particularly when coupled with adaptive optical techniques.[9]

Since it may be impractical in many high power laser applications to achieve either sufficiently large apertures or to produce the uniform or special intensity distributions that minimize thermal blooming, other irradiance-tailoring techniques[10, 11] or phasefront-tailoring techniques[8, 12] may be more useful. Additional work is now in progress in both of these areas.

Acknowledgment

We thank R. M. Szejn for his able assistance with the computer programs employed in this work.

REFERENCES

(To Appendix)

1. J. P. Gordon, C. C. Leite, R. S. Moore, S. P. S. Porto, and J. R. Whinnery, J. Appl. Phys. 36, 3 (1965).

2. A concise review of this topic for gaseous media is presented in J. N. Hayes, P. B. Ulrich, and A. H. Aitken, Appl. Opt. 11, 257, (1972).

3. P. B. Ulrich, J. Opt. Soc. Am. 64, 549 (1974).

4. L. W. Casperson and M. S. Shekhani, Appl. Opt. 14, 1653 (1975).

5. W. P. Brown, Jr., unpublished.

6. G. D. Boyd and J. P. Gordon, Bell Syst. Tech. J. 40, 489 (1961).

7. G. Goubau and F. Schwering, IRE Trans., Atennnas and Propag. AP-9, 248, (1961).

8. W. B. Bridges and J. E. Pearson, Appl. Phys. Lett. 26, 539 (1975).

9. W. P. Brown, Jr., unpublished.

10. J. Wallace, I. Itzkam, and J. Camm, J. Opt. Soc. Am. 64, 1123 (1974).

11. C. Yeh, J. E. Pearson, and W. P. Brown, Jr., "Enhanced Target Irradiance in the Presence of Thermal Blooming," to appear in Appl. Opt.

12. L. C. Bradley and J. Herrman, Appl. Opt. 13, 331 (1974).

APPENDIX

In this appendix, we derive the normalizations used in the text for the focal-plane irradiance and for the field amplitudes for the various beams in terms of the total laser transmitter power. The total transmitted power is given by

$$P_T = \int_{A_T} |E|^2 \, dA_T = \frac{4\pi}{m+1} \rho_o^2 A_m^2 F_1(a_o/\rho_o) \qquad \text{(A-1)}$$

where A_T is the aperture area, E is the field amplitude as defined in Eq. (1), and F_1 is a constant given by

$$F_1(a_o/\rho_o) = \int_0^{a_o/\sqrt{2}\rho_o} f_m^2(\sqrt{2}\rho_o x)\, x\, dx \, . \qquad \text{(A-2)}$$

The maximum aperture dimension is a_o and ρ_o is the e-folding intensity radius of the Gaussian beam in Eq. (8).

The focal plane irradiance as plotted in Figs. 3 and 6 is found from Eqs. (3) and (4):

$$|u(r_o, \theta_o, z)|^2 = \left[\frac{2\pi \cos(m\theta_o)}{\lambda z}\right]^2 I_m^2(r_o, z) \qquad \text{(A-3)}$$

with I_m defined by Eq. (4). We are interested in the maximum focal-plane irradiance, which will occur at $\theta_o = 0$ and at some r_o, depending on the initial irradiance distribution. Using $\theta_o = 0$ and combining Eqs. (A-2), (A-3), and Eq. (4), the irradiance can be written as

$$|u|^2 = 4\pi(m+1)\left(\frac{\rho_o}{\lambda z}\right)^2 a^{-\alpha z}\ \frac{F_2^2(a_o/\rho_o),\ \alpha)\ P_T}{F_1(a_o/\rho_o)} \qquad \text{(A-4)}$$

where α is the propagation medium absorption, F_1 is defined in Eq. (A-2), and F_2 is given by

$$F_2(a_o/\rho_o,\ \beta) = \int_0^{a_o/\sqrt{2}\,\rho_o} f_m(\sqrt{2}\,\rho_o x)\ J_m(\beta x)\ x\,dx \qquad \text{(A-5)}$$

and

$$\beta = \frac{2\pi\sqrt{2}\ \rho_o\ r_o}{\lambda z}\ . \qquad \text{(A-6)}$$

We have evaluated the integral function F_2 in Eq. (A-5) for each of the 7 radial f_m functions discussed in the text (Eqs. (6)-(12)) to find the maximum value of F_2 as a function of the normalized parameter ρ. The values $a_o/\rho_o = 1.52$, $a_o/b_o = 7$, $r_m/a_o = 2/3$, and $\rho = 1$ were used for this evaluation. Table A-1 gives the results of this analysis. To obtain numerical results, we chose $\lambda = 10.6\ \mu m$, $z = 2$ km, and $\rho_o = 23$ cm (corresponding to $a_o = 35$ cm). The irradiance plotted as the ordinate axes in Figs. (3) and (6) is thus given by

$$|u|^2 = 0.0592\ (m+1)\ \frac{F_2^2}{F_1}\ (\text{S.R.})\ P_T \qquad \text{(A-7)}$$

in units of power per square centimeter, with (S.R.) being the strehl ratio determined by the thermal blooming computer code (S.R. = 1 for free-space propagation). For the blooming calculations, the following parameters were taken:

absorption = 2×10^{-4} m^{-1}

transverse wind velocity = 10 m/sec

beam slew rate = 20 mrad/sec

Table A-1. Values for Peak Focal-Plane Irradiance Calculations

Case	m	F_1	(F_2) max.	(β) max.
Inf. Gaus.	0	0.25	0.50	0
Trunc. Gaus.	0	0.225	0.342	0
II-a	1	0.225	0.167	2.50
II-b	1	0.508	0.279	2.31
III-a	0	0.0509	0.161	0
III-b	0	0.508	0.536	0
III-c	0	0.566	0.566	0
III-d	0	0.214	0.331	0

REFERENCES

(To Text)

1. J. E. Pearson, K. M. Brown, R. G. Finucane, M. L. Minden, K. D. Price, and C. Yeh, "Multidither Adaptive Algorithms," Contract F30602-76-C-0022, Quarterly Technical Report No. 1, Dec. 1975.

2. W. B. Bridges et al., "Coherent Optical Adaptive Techniques (COAT)," RADC-TR-74-38, Oct. 1973.

3. S. Hansen, Unpublished.

4. J. E. Pearson and S. Hansen, "Experimental Studies of a Deformable Mirror Multidither COAT System," submitted to J. Opt. Soc. Am., July 1976.

5. T. R. O'Meara, "Multidither COAT Systems Operating with Deformable Mirrors," submitted to J. Opt. Soc. Am., July 1976.

6. F. G. Gebhardt and D. C. Smith, Appl. Opt. 11, 244 (1972).

7. J. E. Pearson, W. P. Brown, Jr., S. A. Kokorowski, M. E. Pedinoff, and C. Yeh, "COAT Measurements and Analysis," RADC-TR-76-55, March 1976.

8. M. E. Pedinoff, S. A. Kokorowski, "COAT/Target-Signature Interactions," RADC-TR-76-230, July 1976.